National Library of Canada
Acquisitions and Bibliographic Services Branch
395 Wellington Street
Ottawa, Ontario
K1A 0N4

Bibliothèque nationale du Canada
Direction des acquisitions et des services bibliographiques
395, rue Wellington
Ottawa (Ontario)
K1A 0N4

Your file Votre référence

Our file Notre référence

NOTICE

The quality of this microform is heavily dependent upon the quality of the original thesis submitted for microfilming. Every effort has been made to ensure the highest quality of reproduction possible.

If pages are missing, contact the university which granted the degree.

Some pages may have indistinct print especially if the original pages were typed with a poor typewriter ribbon or if the university sent us an inferior photocopy.

Reproduction in full or in part of this microform is governed by the Canadian Copyright Act, R.S.C. 1970, c. C-30, and subsequent amendments.

AVIS

La qualité de cette microforme dépend grandement de la qualité de la thèse soumise au microfilmage. Nous avons tout fait pour assurer une qualité supérieure de reproduction.

S'il manque des pages, veuillez communiquer avec l'université qui a conféré le grade.

La qualité d'impression de certaines pages peut laisser à désirer, surtout si les pages originales ont été dactylographiées à l'aide d'un ruban usé ou si l'université nous a fait parvenir une photocopie de qualité inférieure.

La reproduction, même partielle, de cette microforme est soumise à la Loi canadienne sur le droit d'auteur, SRC 1970, c. C-30, et ses amendements subséquents.

Canada

University of Alberta

Bitumen Films on Air Bubble Surfaces and the Stability of Bitumen Drop to Air Bubble Attachment

by

Karen Lee Alexander

A thesis submitted to the Faculty of Graduate Studies and Research in partial fulfillment of the requirements for the degree of Master of Science

Department of Mechanical Engineering

Edmonton, Alberta

Fall, 1995

National Library
of Canada

Acquisitions and
Bibliographic Services Branch

395 Wellington Street
Ottawa, Ontario
K1A 0N4

Bibliothèque nationale
du Canada

Direction des acquisitions et
des services bibliographiques

395, rue Wellington
Ottawa (Ontario)
K1A 0N4

Your file Votre référence

Our file Notre référence

THE AUTHOR HAS GRANTED AN IRREVOCABLE NON-EXCLUSIVE LICENCE ALLOWING THE NATIONAL LIBRARY OF CANADA TO REPRODUCE, LOAN, DISTRIBUTE OR SELL COPIES OF HIS/HER THESIS BY ANY MEANS AND IN ANY FORM OR FORMAT, MAKING THIS THESIS AVAILABLE TO INTERESTED PERSONS.

L'AUTEUR A ACCORDE UNE LICENCE IRREVOCABLE ET NON EXCLUSIVE PERMETTANT A LA BIBLIOTHEQUE NATIONALE DU CANADA DE REPRODUIRE, PRETER, DISTRIBUER OU VENDRE DES COPIES DE SA THESE DE QUELQUE MANIERE ET SOUS QUELQUE FORME QUE CE SOIT POUR METTRE DES EXEMPLAIRES DE CETTE THESE A LA DISPOSITION DES PERSONNE INTERESSEES.

THE AUTHOR RETAINS OWNERSHIP OF THE COPYRIGHT IN HIS/HER THESIS. NEITHER THE THESIS NOR SUBSTANTIAL EXTRACTS FROM IT MAY BE PRINTED OR OTHERWISE REPRODUCED WITHOUT HIS/HER PERMISSION.

L'AUTEUR CONSERVE LA PROPRIETE DU DROIT D'AUTEUR QUI PROTEGE SA THESE. NI LA THESE NI DES EXTRAITS SUBSTANTIELS DE CELLE-CI NE DOIVENT ETRE IMPRIMES OU AUTREMENT REPRODUITS SANS SON AUTORISATION.

ISBN 0-612-06438-7

Canada

University of Alberta

Library Release Form

Name of Author: Karen Lee Alexander

Title of Thesis: Bitumen Films on Air Bubble Surfaces and the Stability of Bitumen Drop to Air Bubble Attachment

Degree: Master of Science

Year this Degree Granted: 1995

Permission is hereby granted to the University of Alberta Library to reproduce single copies of this thesis and to lend or sell such copies for private, scholarly, or scientific research purposes only.

The author reserves all other publication and other rights in association with the copyright in the thesis, and except as hereinbefore provided, neither the thesis nor any substantial portion thereof may be printed or otherwise reproduced in any material form whatever without the author's prior written permission.

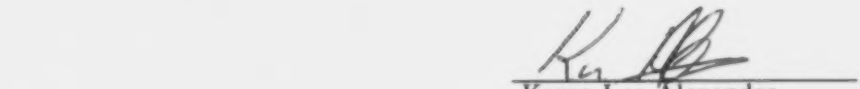

Karen Lee Alexander

11448 - 44A Avenue
Edmonton, Alberta
T6J 0Z9

August 23, 1995

University of Alberta

Faculty of Graduate Studies and Research

The undersigned certify that they have read, and recommend to the Faculty of Graduate Studies and Research for acceptance, a thesis entitled **Bitumen Films on Air Bubble Surfaces and the Stability of Bitumen Drop to Air Bubble Attachment** submitted by Karen Lee Alexander in partial fulfillment of the requirements for the degree of Master of Science.

Dr. D. Li

Dr. J.D. Dale

Dr. J.H. Masliyah

Aug. 2, 1995

ABSTRACT

The dynamic process of bitumen film formation onto an air bubble surface was studied by measuring the time and temperature dependence of bubble surface tension and contact angle. Using an Axisymmetric Drop Shape Analysis technique at 23°C, 50°C, and 70°C showed that the apparent bubble surface tension decreases upon the bitumen - air bubble contact, and gradually reaches a plateau. The time required to reach the final equilibrium value is reduced at higher temperatures. Models were developed in order to estimate the bitumen drop - air bubble attachment stability and bitumen film thickness. The bitumen film thickness for a given air bubble size increases by approximately 140% as temperature is increased from 23°C to 70°C. The bitumen film weakens the attachment by 1 to 10% depending on bitumen drop and air bubble size. In order to enhance bitumen drop - air bubble attachment, the air bubbles and bitumen drops should be the same size.

ACKNOWLEDGEMENT

The author would like to thank Dr. D. Li for his guidance and supervision and the Natural Sciences and Engineering Research Council of Canada for providing postgraduate funding through a PGS A Scholarship.

TABLE OF CONTENTS

CHAPTER 1: INTRODUCTION 1
1.1 Motivation 1
1.2 Bitumen Recovery Process 2
1.2.1 Overview 2
1.2.2 Conditioning 2
1.2.3 Primary Separation 3
1.2.4 Secondary Recovery 3
1.3 Surface Thermodynamics 4
References 10

CHAPTER 2: EXPERIMENTAL EQUIPMENT AND PROCEDURE 11
2.1 Axisymmetric Drop Shape Analysis Profile (ADSA-P) 11
2.1.1 The Principal of ADSA-P 11
2.1.2 Digital Image Processing 13
2.1.3 Drop Profile Analysis 14
2.1.4 Applicability of ADSA-P 16
2.2 Experimental Procedures 17
2.2.1 Methodology 17
2.2.2 Surface Tension Measurements 18
2.2.3 Contact Angle Measurements 19
References 27

CHAPTER 3: EXPERIMENTAL RESULTS 28
3.1 Surface Tension 28
3.2 Contact Angle 30
3.3 Theoretical and Measured Contact Angle Comparison 33
References 42

CHAPTER 4: MODEL OF BITUMEN DROP-AIR BUBBLE ATTACHMENT 43
4.1 Bitumen Drop - Air Bubble Model Formulation 43
4.2 Attachment Model Results 46
References 54

CHAPTER 5: BITUMEN FILM THICKNESS MODEL 55
5.1 Bitumen Film Thickness Model Formulation 55
5.2 Bitumen Film Model Results 59
5.3 Comparison of Bubble Attachment and Bitumen Film Thickness Models 60
References 64

CHAPTER 6: SUMMARY 65
6.1 Summary of Experimental and Model Results 65
6.2 Future Work 66

LIST OF TABLES

Table 3.1: Comparison of theoretical and measured contact angles. 34

Table 5.1: Surface Tension values used to calculate film thickness. 59

Table 5.2: Equilibrium bitumen film thickness to air bubble radius ratio. 60

Table 5.3: Equilibrium bitumen film thickness assuming an air bubble radius of 0.1 mm. 61

LIST OF FIGURES

Figure 1.1: Vapor bubble resting on a solid surface. 9

Figure 1.2: Change in contact radius, dR, with a change in surface area. 9

Figure 2.1: Experimental set-up block diagram. 22

Figure 2.2: Surface tension measurement test cell. 23

Figure 2.3: Typical pendent bubble used for surface tension measurement. 24

Figure 2.4: Contact angle measurement test cell. 25

Figure 2.5: Sessile Bubble for Contact Angle Measurement. 26

Figure 3.1: Time dependence of apparent surface tension of air bubbles with a bitumen film at 23°C. 35

Figure 3.2: Time dependence of apparent surface tension of air bubbles with a bitumen film at 50°C. 36

Figure 3.3: Time dependence of apparent surface tension of air bubbles with a bitumen film at 70°C. 37

Figure 3.4: Time dependence of water-bitumen contact angle at 23°C. 38

Figure 3.5: Time dependence of water-bitumen contact angle at 50°C. 39

Figure 3.6: Air bubble engulfed in bitumen during 70°C contact angle measurement test using a thick bitumen coating on a plastic slide. . . . 40

Figure 3.7: Time dependence of water-bitumen contact angle at 70°C using a thin coating of bitumen on a plastic slide. 41

Figure 4.1: Bitumen drop - air bubble attachment model to predict stability. 48

Figure 4.2: Side view of an axisymmetric air bubble on a bitumen coated surface. .49

Figure 4.3: Bitumen drop - air bubble attachment parameter, h/R_b, as a function of water-bitumen contact angle. 50

Figure 4.4: Effects of the bitumen film on bitumen drop-air bubble attachment at 23°C. 51

Figure 4.5 Effects of the bitumen film on bitumen drop - air bubble attachment at 50°C. 52

Figure 4.6: Effects of the bitumen film on bitumen drop - air bubble attachment at 70°C. 53

Figure 5.1: Two interfaces formed by a bitumen film of thickness h_f on an air bubble surface in water. 63

CHAPTER 1

INTRODUCTION

1.1 MOTIVATION

The spreading of a bitumen film on an air bubble surface is a phenomena which occurs in the secondary recovery stage of the Hot Water Extraction Process used to recover bitumen from oil sands. During the aeration or bubble floatation process which occurs in this stage, a bitumen film spreads over the surface of an air bubble when the air bubbles come into contact with bitumen drops. This bitumen film spreads over the surface of the air bubble because the water-air surface tension is higher than the water-bitumen and bitumen-air surface tensions. In the secondary recovery operation, bitumen recovery can be maximized by increasing the amount of bitumen recovered through the air bubble floatation process. The knowledge of bitumen drop - air bubble interactions and surface properties involved in this operation, such as interfacial tensions and contact angles, will contribute to the optimization of recovery techniques and operating conditions.

The formation of a bitumen film on an air bubble surface during the bubble floatation process will change the bubble surface tension and the water-bitumen contact angle, therefore affecting the attachment of a bitumen drop to an air bubble and the thickness of the bitumen film on the air bubble surface. Previous studies have reported bitumen-air and bitumen-water surface tensions [AOSTRA, 1984; AOSTRA, 1989; Potoczny et al., 1984], but none have reported the surface tension of an air bubble with

a bitumen film. The purpose of this investigation was to study the effects of the bitumen film on the surface tension and contact angle of an air bubble in water. The dynamic process of bitumen film formation onto an air bubble surface was studied by measuring the time and temperature dependence of bubble surface tension and contact angle. The experimental results were used in models to predict the stability of the bitumen drop - air bubble attachment and the thickness of the bitumen film on the air bubble surface.

1.2 BITUMEN RECOVERY PROCESS

1.2.1 Overview

The general steps involved in recovering bitumen from surface mined tar sands are: tar sands mining, bitumen and diluent recovery, and bitumen upgrading. The bitumen recovery step is the focus of this thesis. The most common method for recovering bitumen from oil sands is the Hot Water Extraction Process which can be separated into 6 major operations: conditioning, primary separation, secondary recovery, froth treatment, diluent recovery, and tailings disposal [AERCB Vol. II, 1984]. Secondary recovery is the operation which is pertinent to this investigation, therefore, a summary of the first three operations of the Hot Water Extraction Process, as outlined in the literature [AERCB Vol. II, 1984; AERCB Vol.III, 1984], will be summarized.

1.2.2 Conditioning

In this first stage of the process, surface mined oil sands are mixed in a rotating

drum with hot water, caustic soda, and steam to produce a slurry of sand, oil, and water. This process is carried out at a temperature of approximately 80°C and a pH between 8.5 and 9.0. The slurry is then passed through vibrating screens to remove rocks and unbroken lumps of oil sand. The slurry is then pumped into primary separation vessels.

1.2.3 Primary Separation

In the primary separation stage, the slurry from the conditioning stage is pumped into separation cells where, due to natural aeration that occurs in the conditioning stage, dispersed bitumen with attached air bubbles rises to the surface of the cells as a froth. This bitumen is collected in lauders and sent for deaeration and treatment. This is the major source of bitumen recovery in the Hot Water Extraction Process. Coarse solids settle to the bottom of the separation cells and are removed and pumped to the tailings area for disposal. The central zone of the primary separation cell contains bitumen and suspended solids, known as middlings, with insufficient buoyancy to float to the top as a froth. The middlings are withdrawn from the centre of the separation cells and treated in the secondary recovery stage.

1.2.4 Secondary Recovery

In this stage of the Hot Water Extraction Process, the middlings stream, consisting of fine mineral and bitumen from the primary separator, is pumped into a froth floatation cell where it is agitated and aerated. Bitumen floats to the top of the cell and is removed for further conditioning. A solids stream is removed from the bottom of the

cell and sent to the tailings area. This solids stream is a source of unrecovered bitumen due to inefficiencies of the secondary recovery stage. Surface tensions and contact angles are parameters which affect the amount of bitumen recovered during the air bubble floatation process. By increasing the efficiency of the secondary recovery stage, the overall recovery of the Hot Water Extraction Process can be increased. Therefore, the effects of surface phenomenon on the air floatation process is the focus of this investigation.

1.3 SURFACE THERMODYNAMICS

As mentioned in the previous section, the parameters of surface tension and contact angle play an important role in optimizing the secondary recovery stage of the Hot Water Extraction Process. These parameters are part of a larger field of study known as surface thermodynamics. Definitions of surface tension and contact angle will be presented in this section along with derivations of the Laplace and Young equations using basic surface thermodynamic principles.

Just as the energy form of the fundamental equation for a bulk phase can be written in terms of internal energy, U, entropy, S, volume, V, and mole numbers, N [Callen, 1985]:

$$U = U(S, V, N_1, N_2, \ldots, N_r) \tag{1.1}$$

the energy form of the fundamental equation for a surface phase can be written in terms of surface internal energy, U^A, surface entropy, S^A, surface area, A, and surface mole numbers, N^A:

$$U^A = U^A(S^A, A, N_1^A, \ldots, N_r^A) \tag{1.2}$$

In differential form, equation (1.2) can be written as:

$$dU^A = TdS^A + \gamma dA + \sum \mu_i dN_i^A \tag{1.3}$$

where temperature, T, surface tension, γ, and electrochemical potential, μ, are intensive properties. Surface tension may be mathematically defined from this equation as:

$$\gamma = \textit{surface tension} = \left(\frac{\partial U^A}{\partial A}\right)_{S^A, N_i^A} \tag{1.4}$$

Surface tension is analogous to pressure in a three dimensional bulk phase and may be defined as the free energy per unit area of a surface or the force which minimizes surface area. Surface tension may also be defined as the reversible work involved in creating a unit area of new surface at constant temperature, volume, and total number of moles [Blakely, 1973].

By using a Legendre Transformation, the energy form of the fundamental Equation (1.1) can be written as the grand canonical thermodynamic potential, Ω, as follows:

$$\Omega^A = U^A - TS^A - \sum \mu_i N_i \tag{1.5}$$

An illustration of a vapor bubble resting on a solid surface can be seen in Figure 1.1. The total grand canonical free energy of the bulk phases and interfaces shown in Figure 1.1 can be written as follows:

$$\Omega_{tot} = \Omega_l + \Omega_v + \Omega_s + \Omega_{lv} + \Omega_{sv} + \Omega_{sl} \tag{1.6}$$

Assuming that the solid surface is smooth, homogeneous, isotropic and non-deformable, the above equation can be minimized by implicit differentiation considering that the pressures of the liquid and vapor phases along with the liquid-vapor, solid-vapor, and solid-liquid surface tensions are all constants.

$$d\Omega_{tot} = -P_l dV_l - P_v dV_v + \gamma_{lv} dA_{lv} + \gamma_{sv} dA_{sv} + \gamma_{sl} dA_{sl} \tag{1.7}$$

Considering that the total volume of the liquid and vapor phases is constant:

$$V_l + V_v = constant \tag{1.8}$$

and the total solid-vapor and solid-liquid surface area is constant:

$$A_{sv} + A_{sl} = constant \tag{1.9}$$

Equation (1.7) can be written as follows:

$$d\Omega_{tot} = (P_v - P_l)\, dV_l + \gamma_{lv} dA_{lv} + (\gamma_{sl} - \gamma_{sv})\, dA_{sl} \tag{1.10}$$

Given that the liquid-vapor surface area is a function of the volume of the liquid phase and the solid-liquid surface area, the following equation can be written:

$$dA_{lv} = \left(\frac{\partial A_{lv}}{\partial V_l}\right) dV_l + \left(\frac{\partial A_{lv}}{\partial A_{sl}}\right) dA_{sl} \tag{1.11}$$

In order for the total free energy to be minimized, Equation (1.10) must be equal to zero. Substituting Equation (1.11) into Equation (1.10) and equating to zero leads to the equation:

$$d\Omega_{tot} = [-(P_l - P_v) + \gamma_{lv}(\frac{\partial A_{lv}}{\partial V_l})]dV_l + \gamma_{lv}[\frac{\partial A_{lv}}{\partial A_{sl}} - (\gamma_{sv} - \gamma_{sl})]dA_{sl} = 0 \quad (1.12)$$

Since the volume of the liquid phase, V_l, and the solid-liquid surface area, A_{sl}, are independent variables, each of the two terms in Equation (1.12) have to independently be equal to zero. Setting the first term of Equation (1.12) equal to zero results in the Laplace equation of capillarity:

$$P_l - P_v = \gamma_{lv}(\frac{\partial A_{lv}}{\partial V_l}) \quad (1.13)$$

The mean curvature of the liquid-vapor interface, J_{lv}, can be written for the as follows:

$$J_{lv} = \frac{\partial A_{lv}}{\partial V_l} \quad (1.14)$$

therefore, Equation (1.13) can then be written in the form:

$$P_l - P_v = \gamma_{lv} J_{lv} \quad (1.15)$$

If the second term in Equation (1.12) is set equal to zero, Young's equation is obtained:

$$\gamma_{lv}(\frac{\partial A_{lv}}{\partial A_{sl}}) = \gamma_{sv} - \gamma_{sl} \quad (1.16)$$

When a vapor bubble is resting on a solid surface, the angle formed between the liquid-solid interface and the tangent to the liquid-vapor interface at the solid-liquid-vapor three phase contact line is defined as the contact angle, θ. Figure 1.2 shows a change in the vapor bubble contact radius, dR, on the solid surface with respect to a change in surface

area. An increase in the vapor bubble contact radius results in a decrease in the solid-liquid surface area which can be expressed as:

$$dA_{sl} = -2\pi R dR \tag{1.17}$$

The change in liquid-vapor surface area, dA_{lv}, can then be expressed as:

$$dA_{lv} = 2\pi R\cos(\pi-\theta)dR \tag{1.18}$$

Dividing Equation (1.18) by Equation (1.17) and simplifying results in the equation:

$$\frac{dA_{lv}}{dA_{sl}} = \cos\theta \tag{1.19}$$

Substituting Equation (1.19) into Equation (1.16) gives the more commonly recognized form of the Young equation:

$$\gamma_{lv}\cos\theta = \gamma_{sv} - \gamma_{sl} \tag{1.20}$$

The Laplace equation of capillarity (1.15) and Young's equation (1.20) are the two basic equations used in the theoretical models of this investigation.

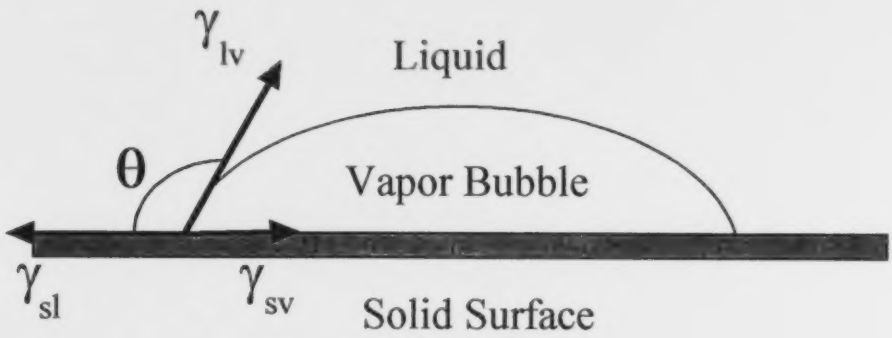

Figure 1.1: Vapor bubble resting on a solid surface.

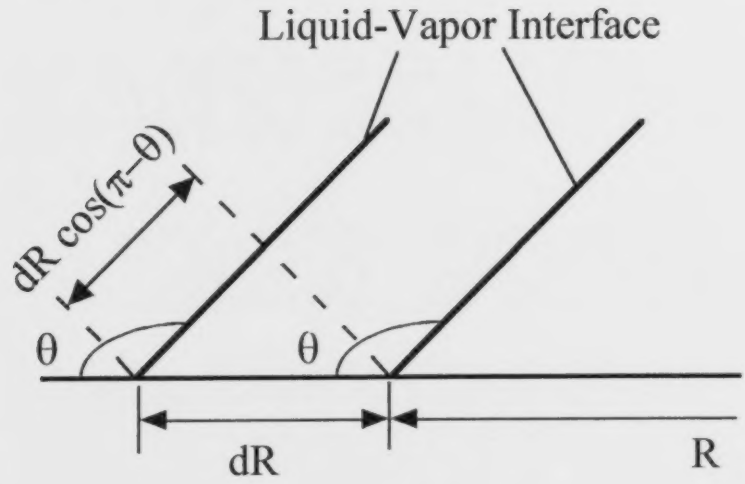

Figure 1.2: Change in contact radius, dR, with a change in surface area.

REFERENCES

Alberta Energy Resources Conservation Board, *Oil Sands Bitumen Extraction Process Evaluation, Volume II, Preliminary Technical Evaluation, Final Public Report,* February 1984.

Alberta Energy Resources Conservation Board, *Oil Sands Bitumen Extraction Process Evaluation, Volume III, Detailed Evaluation of Selected Processes, Final Public Report,* February 1984.

Alberta Oil Sands Technology and Research Authority, *AOSTRA Technical Handbook on Oil Sands, Bitumens and Heavy Oils,* 1989.

Alberta Oil Sands Technology and Research Authority, *The Thermodynamic and Transport Properties of Bitumens and Heavy Oils,* July 5, 1984.

Blakely, J.M., *Introduction to the Properties of Crystal Surfaces,* Peragamon Press, Oxford, 1973.

Callen, H.B., *Thermodynamics and an Introduction to Thermostatistics*, 2nd Edition, John Wiley & Sons, New York, 1985.

Potoczny, Z.M., Vargha-Butler, E.I., Zubovits, T.K., and Neumann, A.W., *AOSTRA Journal of Research,* 1 (1984) 107.

CHAPTER 2

EXPERIMENTAL EQUIPMENT AND PROCEDURE

2.1 AXISYMMETRIC DROP SHAPE ANALYSIS - PROFILE (ADSA-P)

2.1.1 The Principal of ADSA-P

There are many techniques available for measurement of liquid surface tensions and contact angles. Of all the methods which have been developed, the pendent and sessile drop methods are the most general experimental techniques. In addition to the simplicity of using pendent and sessile drops for determining surface tensions and contact angles, these two techniques require only small quantities of liquid and solid surface and they can be used to study both liquid-vapor and liquid-liquid surface tensions. Conventional methods such as the Wilhelmy Plate method could not be used in this investigation of a bitumen film on a liquid-vapor interface because the bitumen film would adhere to the solid surface. The following sections are a brief summary of the technique used in this investigation to study surface tensions and contact angles as outlined in the literature [Li et al., 1992].

To measure the surface tension of pendent bubbles and the contact angle of sessile bubbles, the Axisymmetric Drop Shape Analysis - Profile (ADSA-P) technique was used. ADSA-P is a numerical procedure to digitize images of pendent and sessile drops and bubbles and then to fit Laplacian curves through these digitized profiles with surface tension and contact angle as adjustable parameters. The input for the ADSA-P program

is the density difference between air bubble and the water surrounding the drop; the output of the ADSA-P program consists of the values of surface tension, contact angle (for sessile bubbles), volume of the bubble, liquid-air interface, area and the contact radius of the bubble (for sessile bubbles). Compared with other techniques to measure contact angles and surface tensions from sessile and pendent drops and bubbles, the ADSA-P program has higher accuracy and is essentially free of operator subjectivity. [Cheng et al., 1990]

Axisymmetric Drop Shape Analysis-Profile is a technique to determine liquid-fluid interfacial tensions and contact angles from the shape of axisymmetric menisci. The strategy employed is to construct an objective function which expresses the deviation of the physically observed curve from a theoretical Laplacian curve, ie., a curve satisfying the Laplace equation of capillarity. The objective function is the sum of the squares of the normal distances between the measured points on the pendent or sessile bubble profile and the calculated curve using the Laplace equation. The objective function is minimized numerically with the liquid surface tension as one of the adjustable parameters. The Laplace equation, as described in Chapter 1, is the mechanical equilibrium condition for two homogeneous fluids separated by a curved interface [Bashforth et al., 1883] . This equation relates the pressure difference across a curved interface to the surface tension and the curvature of the interface:

$$\Delta P = \gamma J \tag{2.1}$$

where γ is the interfacial tension, J is the mean curvature of the interface, and ΔP is the pressure difference across the interface. In the absence of external forces other than

gravity, the pressure difference is a linear function of the elevation:

$$\Delta P = (\Delta\rho) g z + \Delta P_o \qquad (2.2)$$

where ΔP_o is the pressure difference at the apex of the drop or bubble, $\Delta\rho$ is the density difference between the two bulk phases, g is the gravitational acceleration and z is the vertical height measured from the apex.

The minimization of the objective function leads to a system of nonlinear equations which are solved using the Newton-Raphson method with incremental loading. A second order implicit Euler method is used to perform the numerical integration. [Cheng et al., 1990; Rotenberg et al., 1983]

Apart from local gravity and densities of the liquid and fluid phases, the only information required by ADSA-P is several arbitrary but accurate coordinate points selected from the drop profile. To achieve rapid and accurate data acquisition and preprocessing, an automatic digitization technique is used [Cheng et al., 1990]. A Fortran computer program was developed in a Ph.D. thesis at the University of Toronto to implement this method [Cheng, 1990].

2.1.2 Digital Image Processing

The drop profile coordinates required by the ADSA-P program are obtained using digital image processing. A video camera produces a video signal containing image data. The signal is transmitted to the image processor where the analog signal is converted to a digital signal containing the image data in the form of pixels. The digital pixel data are stored in frame memory one frame at a time, with each pixel occupying one frame

memory location. Once the image is stored in frame memory, it may be accessed for display or additional computer processing. Display circuitry transforms the pixels stored in frame memory back into an analog signal for display on a video monitor. The number of pixels that are transferred to or from frame memory in one frame time defines the display resolution of the frame memory. The size of the memory limits the maximum number of pixels stored.

A diagram of the apparatus used in the experiments is shown in Figure 2.1. For both the pendent and sessile bubble experiments, air bubbles were formed in water. In the setup, a Cohu 4910 CCD monochrome camera was mounted on a Leica Wild M3B microscope. For all images, a magnification of 10.08x was used which resulted in a resolution of approximately 10 μm per pixel. The video signal of the pendent or sessile bubble was transmitted to a VideoPix digital video processor which performed the frame grabbing and digitization of the image to 640 by 480 pixels with 256 gray levels each where zero represents black and 255 represents white. A Sun SparcStation 10 Unix computer was used to acquire the image from the image processor and perform the image analysis and computation. Once an image of a drop is stored in memory, the ADSA-P program automatically finds the drop profile coordinates with sub-pixel resolution and corrects for optical distortion due to the camera and lenses.

2.1.3 Drop Profile Analysis

A gradient magnitude method is used to find the bubble profile coordinates. This

method relies on the analysis of small square portions, 3x3 pixel points, of the digitized image. The X and Y coordinates of the pixel points represent two dimensions and the gray level intensity associated with each pixel can be considered as a third dimension. Using an edge operator scheme, the best least-squares plane is fit through nine gray level pixels of the 3x3 array, and then the slope of this plane in the X and Y directions is calculated. From these two directional gradients, the overall gradient of this plane can then be calculated. This gradient represents the gradient of the gray level at the central point of the 3x3 array of pixels. This procedure is then repeated for the whole digitized image such that each pixel point is the central point of the 3x3 array. A gray level gradient for each pixel point of the whole image is therefore established, leading to a gradient image. The bubble profile is approximated by the pixels of steepest gray gradient from outside of the image of the bubble to the inside, through the boundary. Once the bubble profile coordinates have been determined, ADSA-P selects 20 points at random from the bubble profile and solves for surface tension or contact angle. This process is repeated 10 times leading to average values with corresponding 95% confidence limits for all output parameters [Cheng, 1990].

The camera produces slightly distorted images which can cause major errors in the final results of surface tension and contact angle. After images of the bubbles were taken during each experiment, an image of a calibration grid pattern on an optical glass was taken at the same camera position. The grid is used for both correction of the optical distortion and calibration. The image of the grid is established by the coordinates of the intersection points of the horizontal and vertical grid lines. Each intersection point

is calculated from the intersection of two perpendicular lines formed by finding the "darkest" pixels, i.e., the pixels of lowest gray level, on the nearby horizontal and vertical grid lines. Each grid is approximately 1 pixel wide. The distorted grid is then mapped onto the known undistorted grid. Hence, the distortion of all drop images is corrected during the mapping of the grid. The advantage of this method is that the aspect ratio of the digitized board does not have to be known. The accuracy of this correction is ± 1 pixel.

2.1.4 Applicability of ADSA-P

The applicability of ADSA-P ranges from ultra low surface tensions in the range of 10^{-2} to 10^{-4} mJ/m^2 [Boyce et al., 1984] to drops of liquid metals in an ultra high vacuum at 1000's of mJ/m^2. If a pendent drop method is used, an accurate value liquid-fluid surface tension can be calculated using ADSA-P because no surface effects are present. If a sessile drop is used, ADSA-P can calculate both surface tension and contact angle simultaneously. Using a homogeneous smooth and flat surface, contact angles accurate to $\pm 0.1^{\circ}$ can be obtained. For sessile drops which have very low contact angles below 20°, the precision of ADSA-P decreases because it becomes difficult to acquire accurate coordinate points along the edge of the drop profile. An Axisymmetric Drop Shape Analysis - Contact Diameter (ADSA-CD) program was developed for this situation [Skinner et al., 1989].

2.2 EXPERIMENTAL PROCEDURES

2.2.1 Methodology

In order to study the time and temperature affects of a bitumen film on an air bubble surface, surface tensions and contact angles were measured at three temperatures: 23°C (room temperature), 50°C, and 70°C as a function of time. The experimental procedure was separated into two stages: surface tension measurement using pendent bubbles and contact angle measurement using sessile bubbles. For both stages, Syncrude Feed Bitumen #85-01 was used to form a bitumen film on an air bubble surface surrounded by distilled water. The pH of the distilled water was 7.1 measured using a Fisher Accumet Model 805 MP pH meter.

For the higher temperature tests conducted 50°C, and 70°C, a heating water jacket was designed to heat a square glass beaker test cell using a Haake F2 hot water bath. The water jacket was designed out of steel with one side constructed out of glass to allow a light source to illuminate the test cell. The side opposite to the glass contained a vertical slot in the steel wall in order to view the test cell with the camera and microscope. Prior to the experiments, the square glass beaker was filled with distilled water, covered, and placed in the water jacket. The time to reach a steady test water temperature and difference in temperature between the water bath and test beaker were recorded at temperatures ranging from 30°C to 90°C. The results were used to allow a sufficient heating time to achieve the temperatures of 50°C and 70°C in the test beaker during the actual experiments.

2.2.2. Surface Tension Measurements

Surface tension measurements were carried out at room temperature (23°C), 50°C, and 70°C. A Teflon needle was guided into a square glass beaker with the aid of a metal j-shaped jacket as shown in Figure 2.2. The Teflon needle was connected to a micrometer syringe in order to form air bubbles in the upward direction and the square glass beaker was filled with distilled water. For the increased temperature measurements, as outlined in the previous section, the beaker was covered and placed inside a water jacket which was connected to a water bath to achieve the desired constant temperature during the measurements.

Clean equipment was essential for obtaining accurate results. The Teflon needle was cleaned using a three step process using acetone, methanol and distilled water. A syringe was used to draw 5 cc's of acetone. The Teflon needle was then connected to the syringe and the acetone was flushed through the needle. This procedure was repeated twice. The same procedure was used flush the Teflon needle with methanol. Finally, the Teflon needle was flushed three times with distilled water using the same procedure as acetone and methanol. The distilled water used for rinsing and the distilled water used in the experiments were from the same source.

The square glass beaker in which the experiments were conducted was rinsed with approximately 10 ml of acetone three times, covered with clean tinfoil, placed upside down in a large covered glass beaker and allowed to dry. The metal j-shaped jacket was rinsed using approximately 15 ml of acetone, covered with tinfoil, turned upside down and allowed to dry. Once dry, the Teflon needle was guided into the metal jacket. The

Teflon needle was then connected to the 5 cc syringe and flushed with distilled water twice. During the cleaning process, the tip of the Teflon needle was only in contact with clean tinfoil or the inside of the clean and dry metal jacket.

Before bitumen was added to the system, a room temperature air-water interfacial tension, approximately 72.4 mJ/m^2, was obtained using the ADSA-P technique. For the 50°C and the 70°C tests, the distilled water was then heated for one and two hours respectively. Syncrude Feed Bitumen #85-01 was then spread around the tip of the Teflon needle. An air bubble was formed using the micrometer syringe and the camera was focused. A sequential image grabbing program was used to grab images of the air bubble over a period of time until the surface tension values, as determined using ADSA-P, reached an equilibrium value. Initially, images were taken every 3 to 5 seconds. The time interval between images gradually increased to approximately 15 minutes towards the end of each test. A typical air bubble analyzed using this method is shown in Figure 2.3.

2.2.3 Contact Angle Measurements

The contact angle experiments were also carried out at room temperature, 50°C, and 70°C. In order to obtain contact angle values, a surface of bitumen was prepared. Syncrude Feed Bitumen #85-01 was dissolved in toluene and poured into petri dishes containing smooth glass slides which had been cleaned in 15 ml of acetone and allowed to dry. The glass slides covered in the bitumen/toluene solution were then baked in an oven at 75°C for 6 hours where the toluene evaporated and the glass slides became coated

with bitumen. The petri dishes were taken out of the oven, covered, and allowed to cool for a minimum of 12 hours. Using clean forceps, the bitumen coated glass slides were removed from the petri dish and immersed in a clean square glass beaker containing distilled water. As with the higher temperature surface tension measurements, the beaker was covered and placed in a water jacket and heated using a water bath calibrated using the method as described in Section 2.2.1.

Figure 2.4 shows the test cell used to measure the contact angle of a sessile air bubble resting on a bitumen coated slide. Air bubbles were formed on the bitumen coated slides from above using a clean Teflon needle guided by a clean straight metal jacket. Once again, the Teflon needle was connected to a micrometer syringe. Air bubbles attached to the tip of the Teflon needle were placed in contact with the bitumen surface. The volume of the air bubble was increased using the micrometer syringe and the Teflon needle was raised away from the bitumen coated surface. When the Teflon needle was raised, the air bubble would detach from the Teflon needle and stick to the bitumen coated slide. The camera as focused and images of the air bubble on the surface surrounded by water were taken over a period of time using a sequential image grabbing program until the contact angle, as determined by ADSA-P, reached an equilibrium value. Using the same method as in the surface tension time intervals, images of the sessile bubble were taken at shorter time intervals at the beginning of the test than at the end of the test. A typical bubble used to determine contact angle using this technique is shown in Figure 2.5. Note that the contact angle of the air bubble in water in this figure is measured from the bitumen surface through the water phase to the liquid-vapor

interface. Each air bubble was deposited on a different location of the bitumen coated slide for each test.

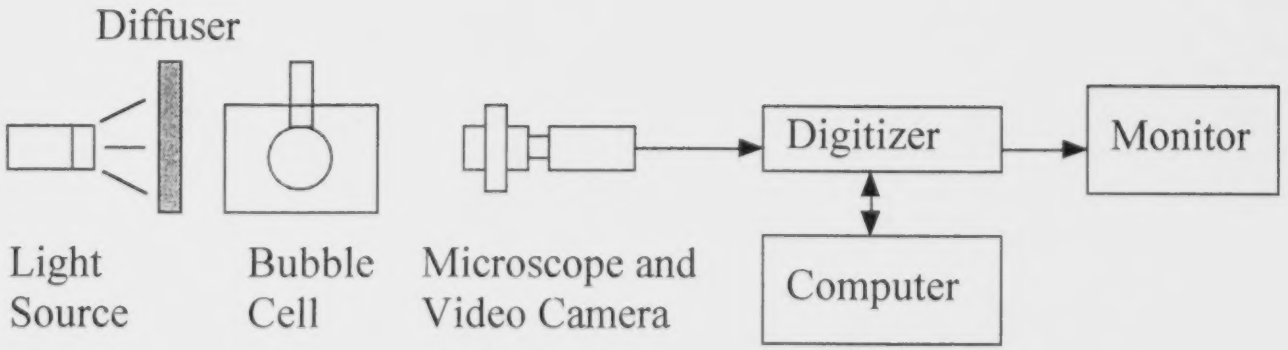

Figure 2.1: Experimental set-up block diagram.

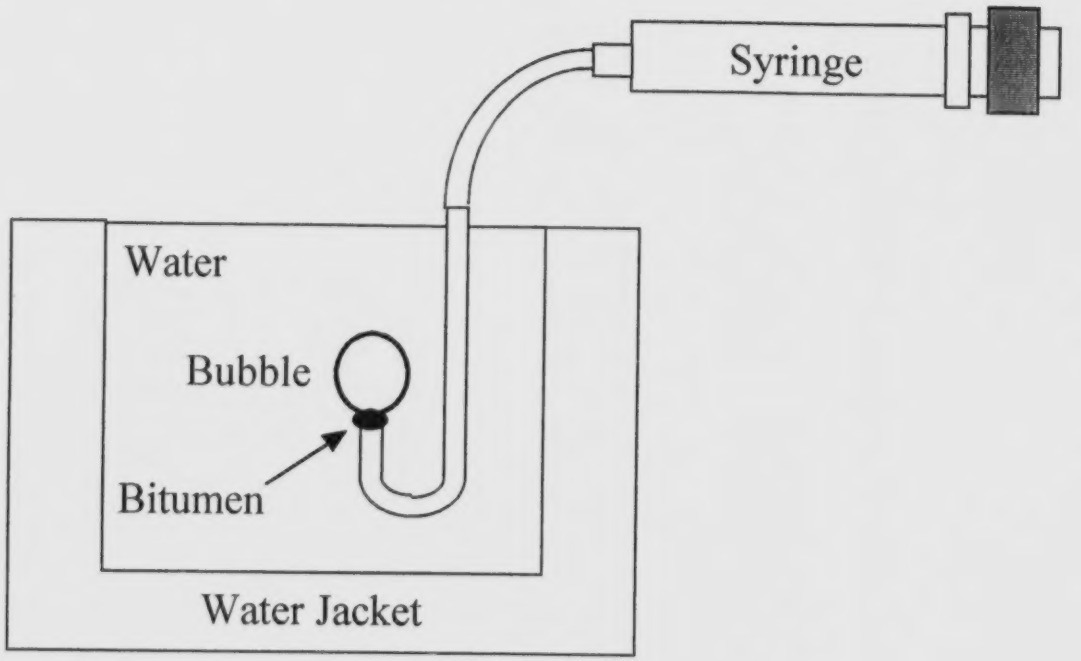

Figure 2.2: Surface tension measurement test cell.

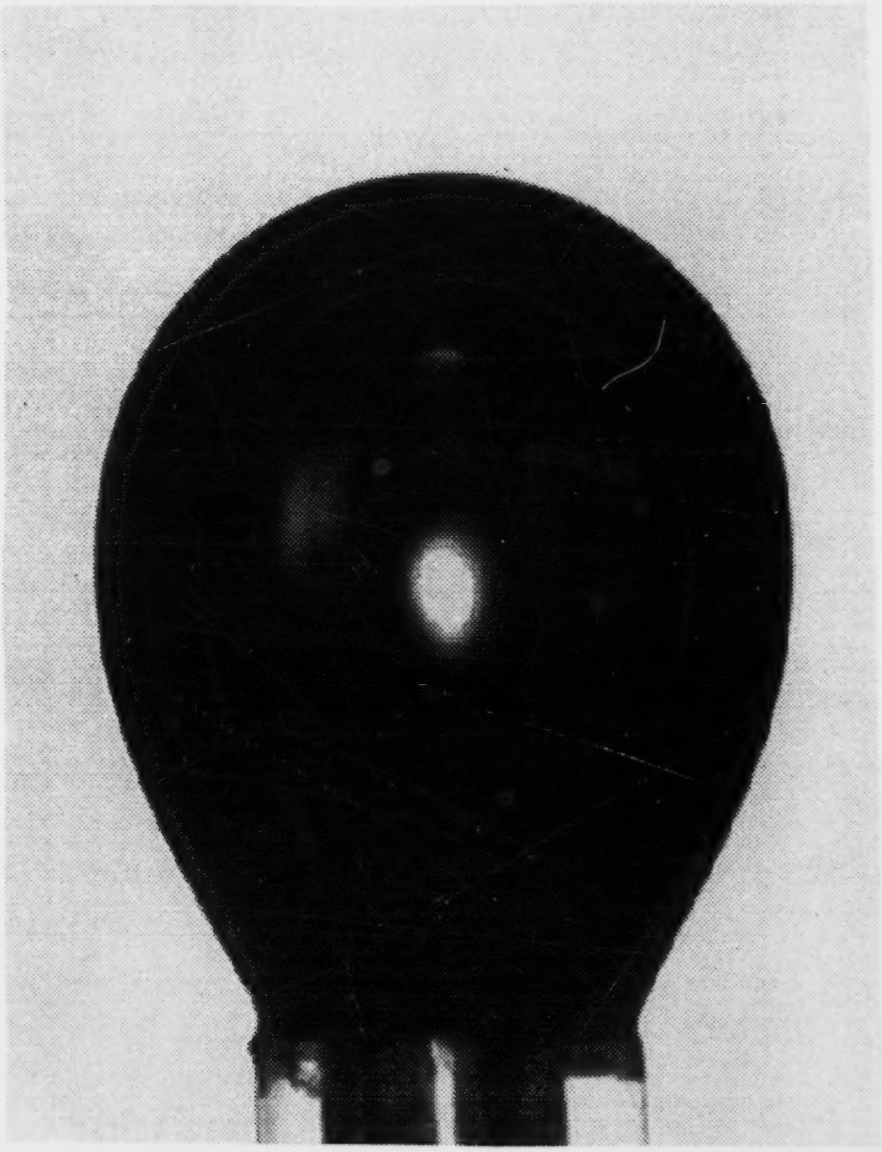

Figure 2.3: Typical pendent bubble used for surface tension measurement.

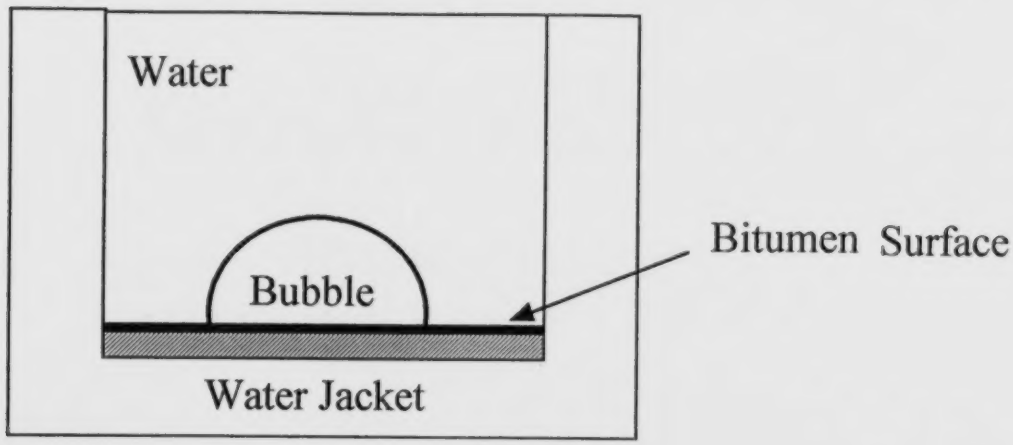

Figure 2.4: Contact angle measurement test cell.

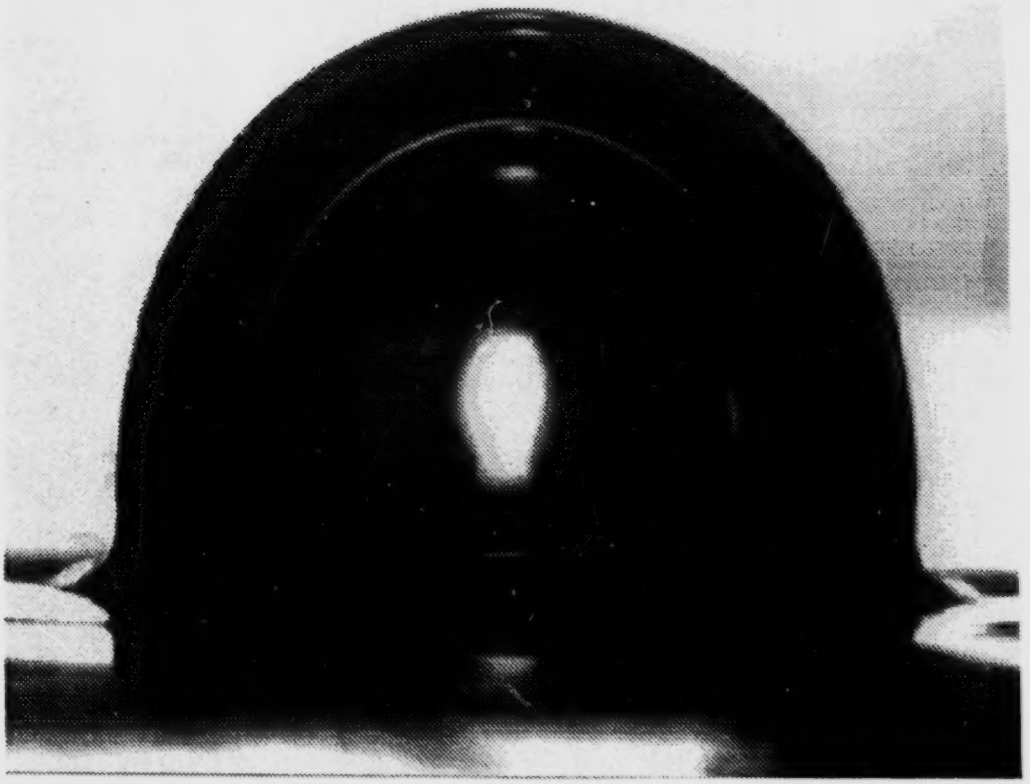

Figure 2.5: Sessile Bubble for Contact Angle Measurement.

REFERENCES

Bashforth F. and Adams, J.C., *An Attempt to test the Theories of Capillary Action*, Cambridge University Press and Deighton Bell & Co, Cambridge, 1883.

Boyce, J.F., Schürch, S., Rotenberg, Y., and Neumann, A.W., *Colloids and Surfaces*, 9 (1984) 307.

Cheng, P., Li, D., Boruvka, L., Rotenberg, U., and Neumann, A.W., *Colloids and Surfaces*, 43 (1990) 151.

Cheng, P., Ph.D. Thesis, University of Toronto, Toronto, Canada, 1990.

Li, D., Cheng, P., and Neumann, A.W., *Advances in Colloid and Interface Science*, 39 (1992) 347.

Rotenberg, Y., Boruvka, L., and Neumann, A.W., *Journal of Colloid and Interface Science*, 93 (1983) 169.

Skinner, F.W., Rotenberg, Y., and Neumann, A.W., *Journal of Colloid and Interface Science*, 130 (1989) 25.

CHAPTER 3

EXPERIMENTAL RESULTS

3.1. SURFACE TENSION

It was observed that immediately after an air bubble was formed with bitumen on the tip of the teflon needle, a bitumen film started to form around the surface of the air bubble causing the surface to discolour. This bitumen film causes a decrease in the initial air-water interfacial tension which eventually reaches a plateau as shown for room temperature, 50°C, and 70°C in Figures 3.1, 3.2, and 3.3 respectively. In these figures, the surface tension of an air bubble surface with a bitumen film is referred to as the apparent surface tension. It was observed during the tests that the thickness of the bitumen film on the air bubble surface increased and the radius of the air bubble decreased as the surface tension approached an equilibrium value. It was also observed that the thickness of the bitumen film on the air bubble surface increased as temperature increased.

Figure 3.1 shows the apparent surface tension time dependence for room temperature. The mean curve shown in Figure 3.1 is an average of five different air bubbles on tests conducted on two separate days. Figure 3.1 shows a rapid decrease in the surface tension followed by a gradual change towards the equilibrium value. The apparent surface tension reached an equilibrium value of 60.7 $\pm$ 1.4 mJ/m^2 after approximately 11 minutes. The equilibrium value for apparent surface tension represents an approximate reduction of 11.7 mJ/m^2 or 16% of the published value for water-air

interfacial tension, 72.4 mJ/m^2, at this temperature [Jasper, 1972]. All values for the means and error estimates were calculated using a t distribution statistical analysis for mean and standard deviation. The equilibrium time was calculated assuming that equilibrium was achieved when the difference between the water-air surface tension and the apparent surface tension was within 1.5% of the difference between the water-air surface tension and the equilibrium mean surface tension. As shown in Figure 3.1, the change of the apparent surface tension with time indicates the process of the bitumen film formation onto the air bubble: the initial rapid decrease of the surface tension corresponds to the initial rapid growth and spreading of a bitumen film; the final equilibrium of the apparent surface tension reflects the equilibrium of the bitumen film.

Figure 3.2 shows the time dependence of the apparent surface tension at a test temperature of 50°C. The mean curve was calculated from tests performed with seven different air bubbles on two different days. The same trend of a rapidly decreasing surface tension followed by an equilibrium value is seen in Figure 3.2. The equilibrium value for apparent surface tension, 57.4 $\pm$ 0.9 mJ/m^2, is approximately 5% lower than the apparent surface tension equilibrium value at room temperature. The apparent surface tension mean value at 50°C is approximately 11.4 mJ/m^2 or 17% lower than the published value for water-air interfacial tension, 68.5 mJ/m^2, at 50°C [Jasper, 1972] . Also noted is the time to reach equilibrium which is now reduced to approximately 2.5 minutes from 11 minutes at room temperature.

The apparent surface tension plot for 70°C is shown in Figure 3.3. The mean curve was calculated from the test results of six separate bubbles on two different days.

At this temperature, the equilibrium value for the apparent surface tension, 56.3 $\pm$ 0.3 mJ/m^2, was reached after approximately 7 seconds. The equilibrium value is 9.2 mJ/m^2 or 14% less than the known water-air interfacial tension, 65.5 mJ/m^2 [Jasper, 1972]. It is clear when comparing this figure to Figures 3.1 and 3.2 that the apparent surface tension of the air bubble with a bitumen film decreases with increasing temperature. It is also evident that the time to reach equilibrium is drastically reduced at higher temperatures. This means that the process of bitumen film formation onto an air bubble surface is much shorter at higher temperatures. Between room temperature and 70°C, there was a 7% reduction in apparent surface tension and a 99% reduction in equilibrium time.

3.2. CONTACT ANGLE

As with the surface tension experiments, a bitumen film was observed to form on the surface of the air bubble as soon as the air bubble contacted the bitumen surface. This resulted in a changing contact angle between the air bubble and the bitumen surface which eventually reached an equilibrium value as shown in Figures 3.4 and 3.5 for room temperature and 50°C respectively. Difficulties were encountered during the tests conducted at 70°C and therefore some inaccuracies may be present in the contact angle data presented for this temperature. These difficulties will be discussed later in this section.

As shown in Figure 3.4 for room temperature, the contact angle rapidly increases and eventually reaches a plateau value of 83.9 $\pm$ 3.1 degrees after approximately 150

minutes or 2.5 hours. The mean curve was calculated from tests using six different bubbles each formed on a different locations of the bitumen coated surface. Due to the greater error in the contact angle measurements when compared to the surface tension measurements, the equilibrium time was calculated by assuming equilibrium was achieved when the difference between the initial value for the contact angle and the measured contact angle was within 4% of the difference between the initial contact angle and the equilibrium mean contact angle. Figure 3.5 shows the time dependence of the contact angle for 50°C. The mean curve was calculated from tests on five separate bubbles formed on different locations of the surface. Figure 3.5 shows an increasing contact angle which peaks and then reduces to a plateau value of 78.9 $\pm$ 2.5 degrees in approximately 60 minutes. From room temperature to 50°C, the equilibrium contact angle was reduced by approximately 5 degrees or 6%. The time to reach equilibrium was reduced by approximately 60%.

Results for the time dependence on contact angle at 70°C were very difficult to obtain. It was observed at this temperature that the bitumen coating would not stick to the glass slide. All of the bitumen would lift off of the glass slide during the 2 hour heating period required in order to obtain constant temperature test conditions. Alternate coating techniques were attempted such as dissolving more bitumen in the toluene before baking and using a longer baking time. None of these techniques were successful. It was thought that due to the wetting nature of water and the non-wetting nature of bitumen at this temperature, the water tends to wet the glass surface and remove the bitumen. An alternate method of using an even coating of bitumen on the

surface of a plastic slide was attempted. The bitumen coating would stick to the plastic slide, but when the air bubble was placed on the solid surface, the bitumen spread over bubble surface quickly and engulfed the air bubble in a few seconds. This resulted in no detectable contact angle as can be shown in Figure 3.6. In order to reduce the thickness of the bitumen film on the plastic slide to avoid the engulfing, the bitumen coating was smeared out over the plastic slide several times during the heating process. This method solved the engulfing problem, and the results for time dependence of the water-bitumen contact angle at a test temperature of 70°C are shown in Figure 3.7. An equilibrium contact angle of 85.7 $\pm$ 3.0 degrees reached in approximately 25 minutes was calculated from tests conducted on seven separate bubbles on different locations on the bitumen coated plastic surface. Note that the value for the equilibrium contact angle at 70°C is larger than the equilibrium contact angles at 23°C and 50°C, 83.9 $\pm$ 3.1 degrees and 78.9 $\pm$ 2.5 degrees respectively. The 70°C equilibrium contact angle does not follow the trends observed with the other contact angles and apparent surface tensions. Since the apparent surface tension decreases with increasing temperature, it is expected that the contact angle will decrease with increasing temperature. This is true for the contact angles at 23°C and 50°C, but not for 70°C. For the apparent surface tensions at 23°C, 50°C and 70°C as well as the contact angles at 23°C and 50°C, it was observed that the uncertainty in the equilibrium value decreased as temperature increased. This also did not occur for the equilibrium contact angle at 70°C. The equilibrium value for contact angle at 70°C may therefore be inaccurate due to two reasons. The first and most obvious reason for inaccuracies is that the surface was not ideally smooth due to

surface roughness caused by the smearing process used during heating. The second potential source of error is that it was observed that after a few minutes during tests at this temperature, the bitumen seemed to bake onto the air bubble surface forming a thin solid film. This did not occur during the surface tension experiments conducted with a pendent drop at this temperature.

3.3 THEORETICAL AND MEASURED CONTACT ANGLE COMPARISON

Given Young's Equation (1.20), it can be seen that the contact angle, θ, can be calculated if the liquid-vapor, solid-liquid, and solid-vapor surface tensions are known. For an air bubble resting on a bitumen coated solid surface in water, the liquid-vapor surface tension will be the apparent surface tension as described in Section 3.1. The solid-liquid and solid-vapor surface tension will then become water-bitumen and bitumen-air surface tensions which can be found from previous studies in the literature [AOSTRA, 1984; Potoczny et al., 1984]. Using Young's equation (1.20) with the measured values for apparent surface tension and published valued for water-bitumen and bitumen-air surface tensions, a theoretical contact angle, θ_{th}, can be compared to the measured contact angle, θ_{meas}, as described in Section 3.2. The results are shown on the following page in Table 3.1. Table 3.1 shows that with the exception of the measured contact angle at 70°C, contact angle decreases as temperature increases. At the test temperatures of 23°C and 50°C, the measured values for contact angles are approximately 8.4 degrees or 11% and 9.1 degrees or 13% larger respectively than the theoretical contact angles at these temperatures. The measured contact angle at 70°C is approximately 20.3 degrees or 31%

Table 3.1: Comparison of theoretical and measured contact angles.

	γ_{ap} (mJ/m^2)	γ_{ba} (mJ/m^2) [Potoczny 1984]	γ_{wb} (mJ/m^2) [AOSTRA 1984]	θ_{th} degrees	θ_{meas} degrees
23°C	60.7±1.4	33.3±0.3	18.1±4.0	75.5±3.9	83.9±3.1
50°C	57.4±0.9	31.2±0.27	11.4±4.0	69.8±4.3	78.9±2.5
70°C	56.3±0.3	29.7±0.26	6.3±4.0	65.4±4.5	85.7±3.0

higher than the theoretical contact angle. Some error is inherent in the theoretical calculations for all of the temperatures because the exact same bitumen was not used for all of the quoted surface tension values. Factors such as the solvent used to extract the bitumen and the bitumen components will affect the surface tensions and therefore the contact angle. This method does, however, give an estimation to see if the measured contact angles, as described in Section 3.2, are reasonable.

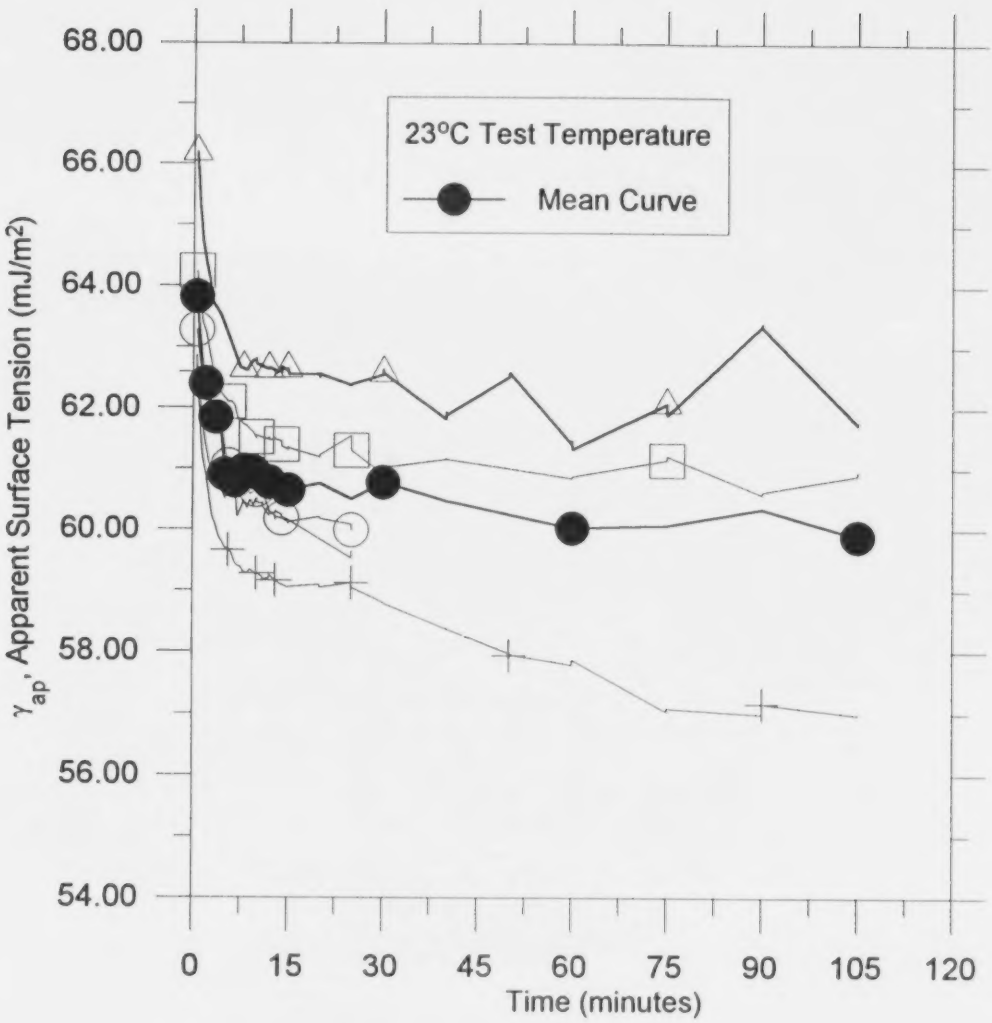

Figure 3.1: Time dependence of apparent surface tension of air bubbles with a bitumen film at 23°C.

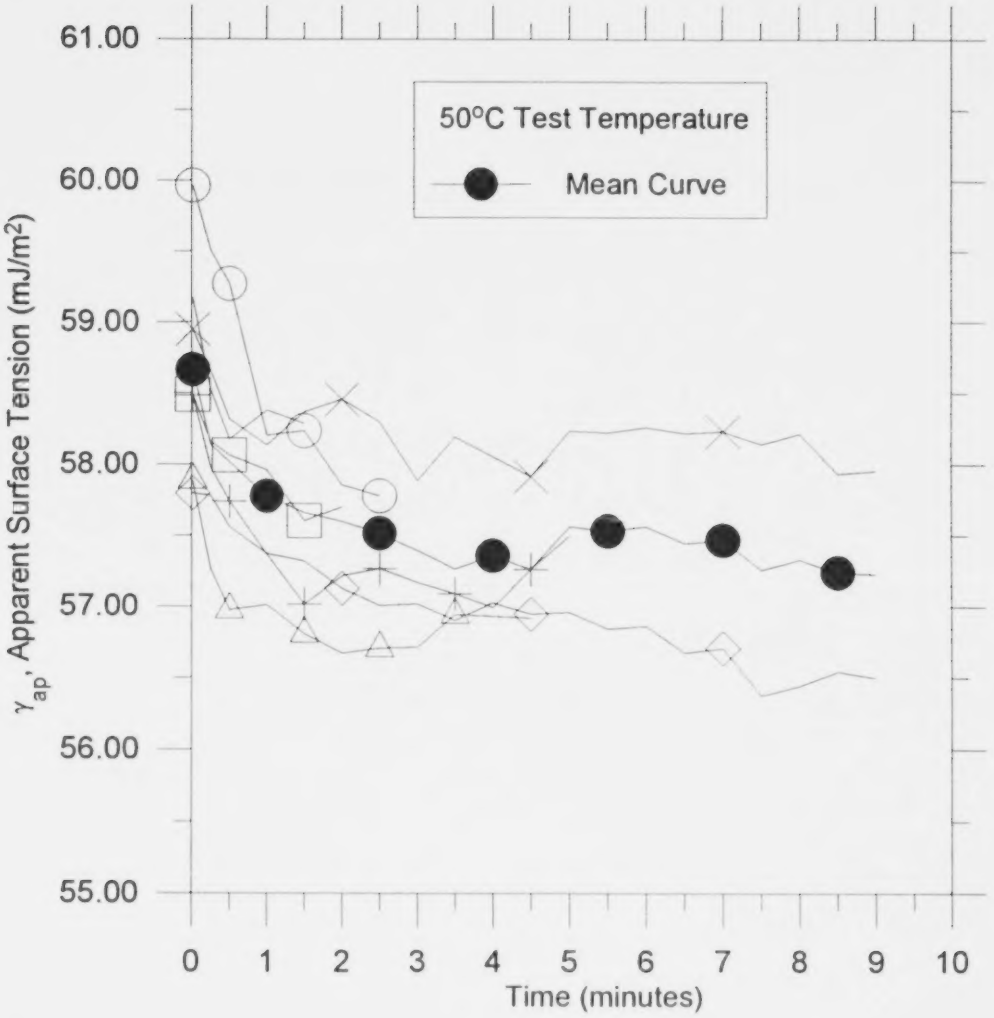

Figure 3.2: Time dependence of apparent surface tension of air bubbles with a bitumen film at 50°C.

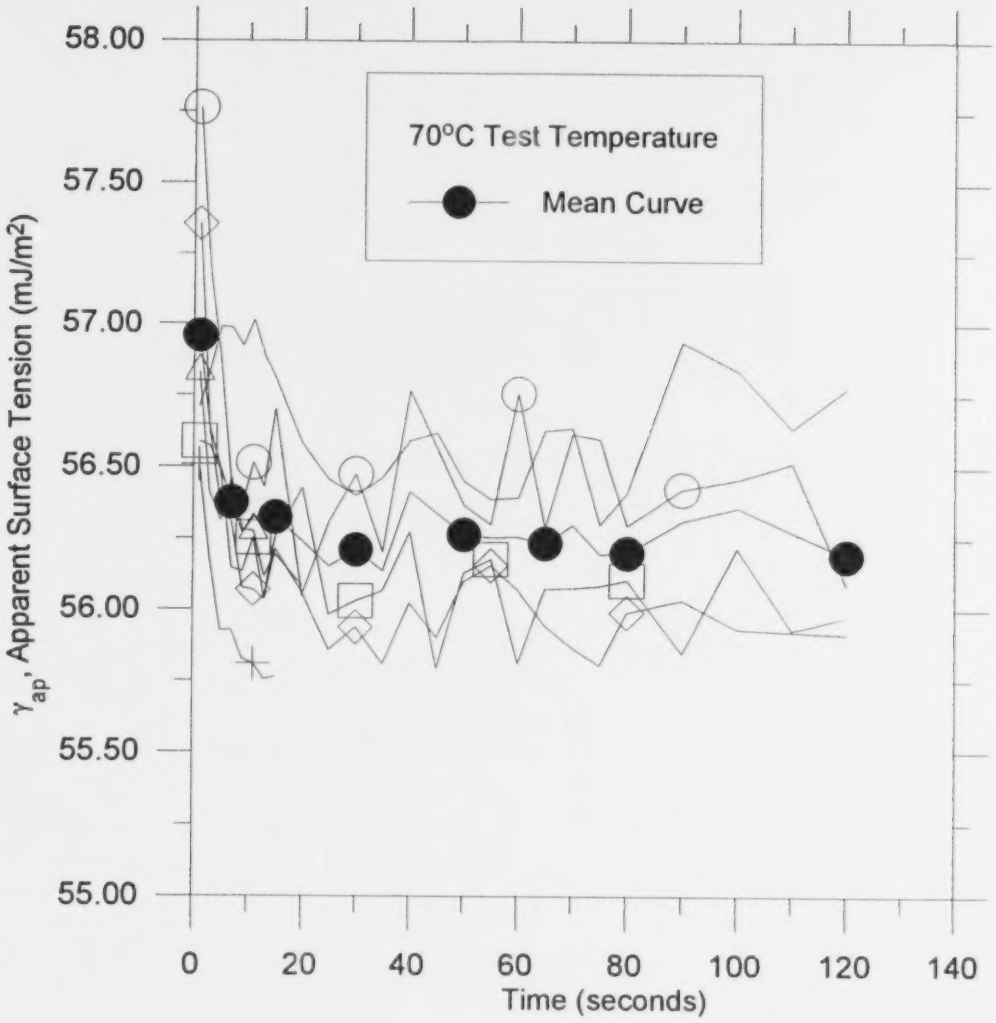

Figure 3.3: Time dependence of apparent surface tension of air bubbles with a bitumen film at 70°C.

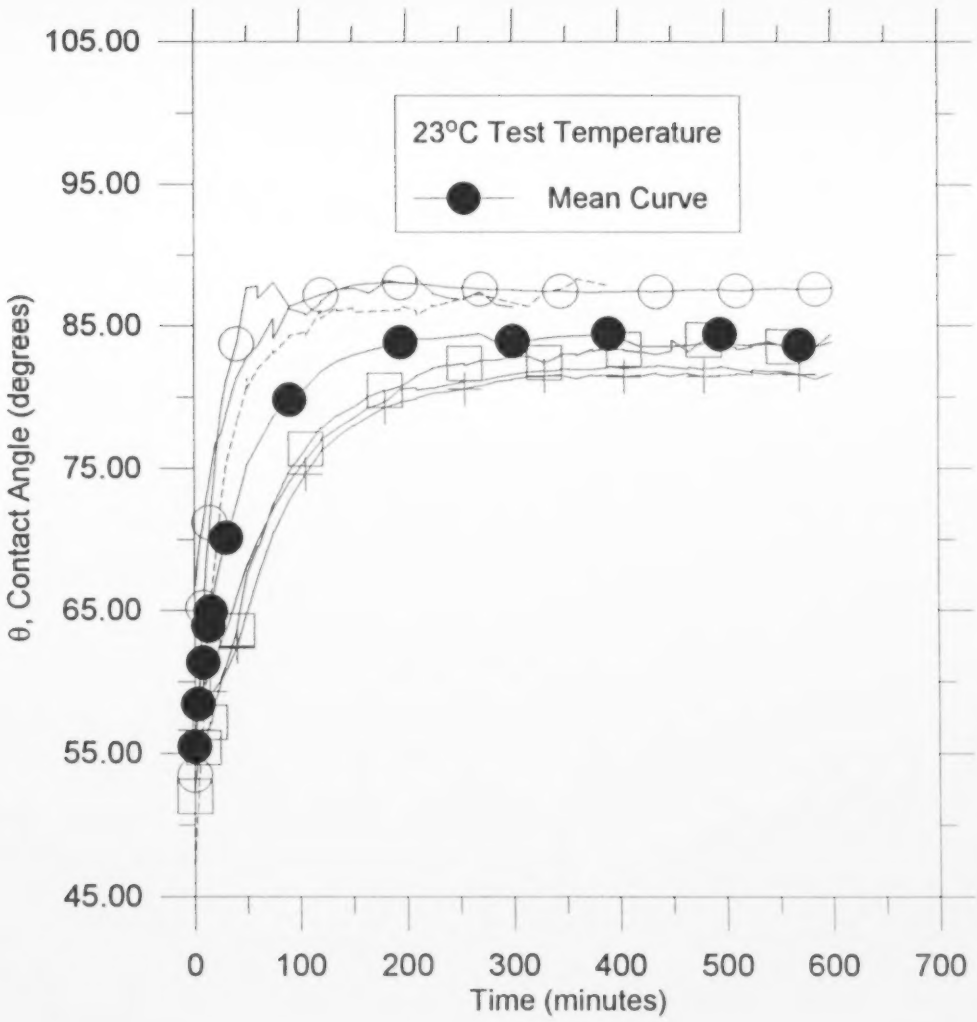

Figure 3.4: Time dependence of water-bitumen contact angle at 23°C.

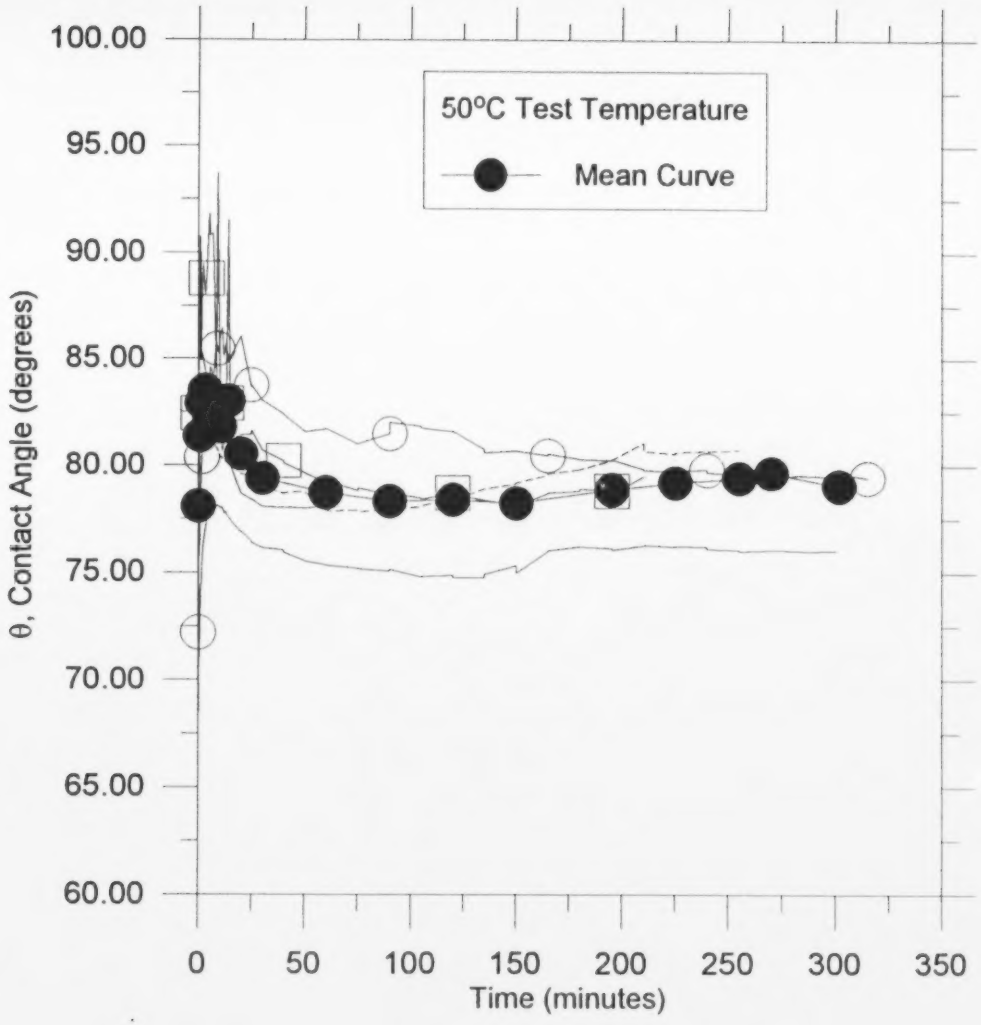

Figure 3.5: Time dependence of water-bitumen contact angle at 50°C.

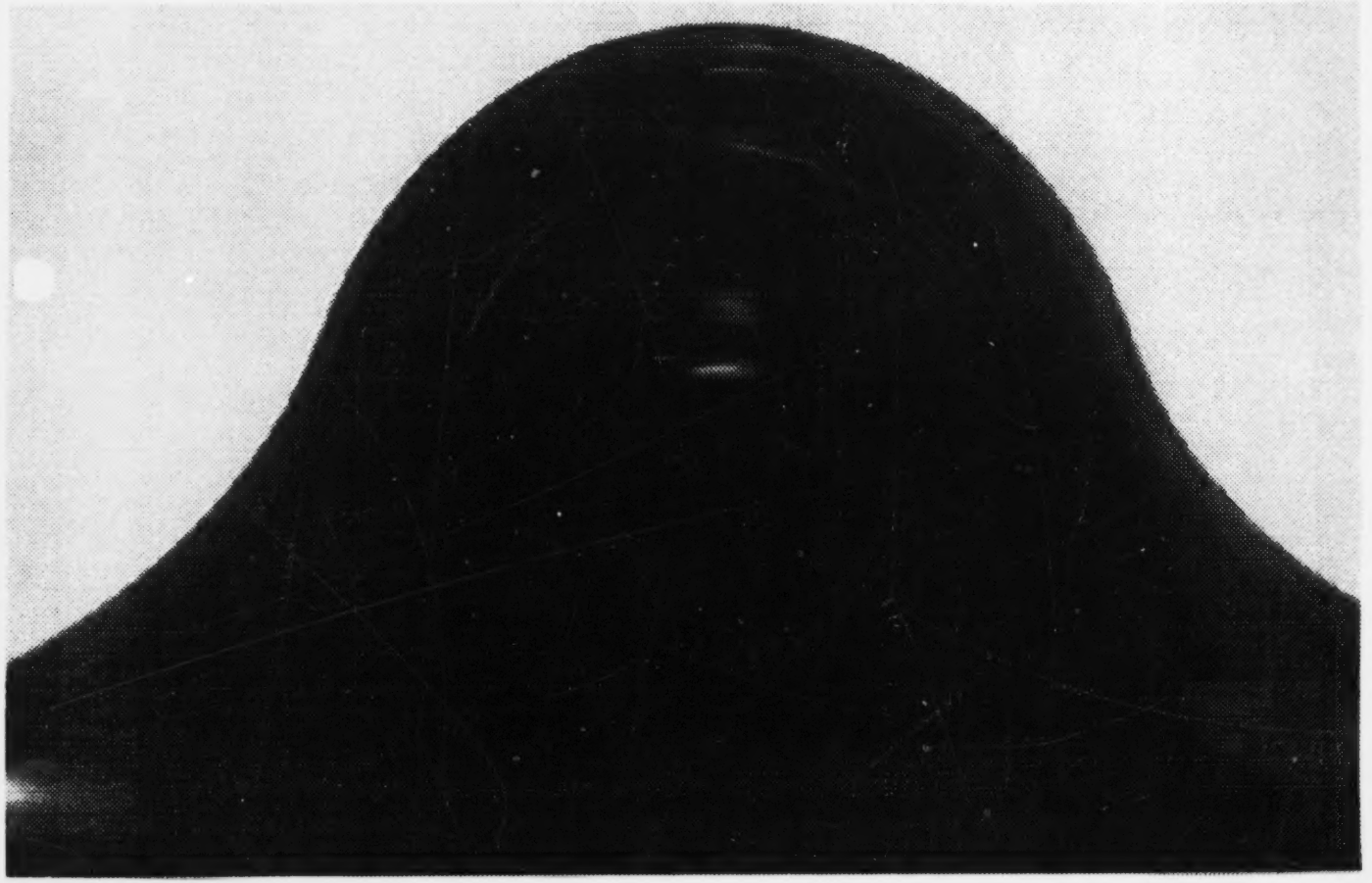

Figure 3.6: Air bubble engulfed in bitumen during 70°C contact angle measurement test using a thick bitumen coating on a plastic slide.

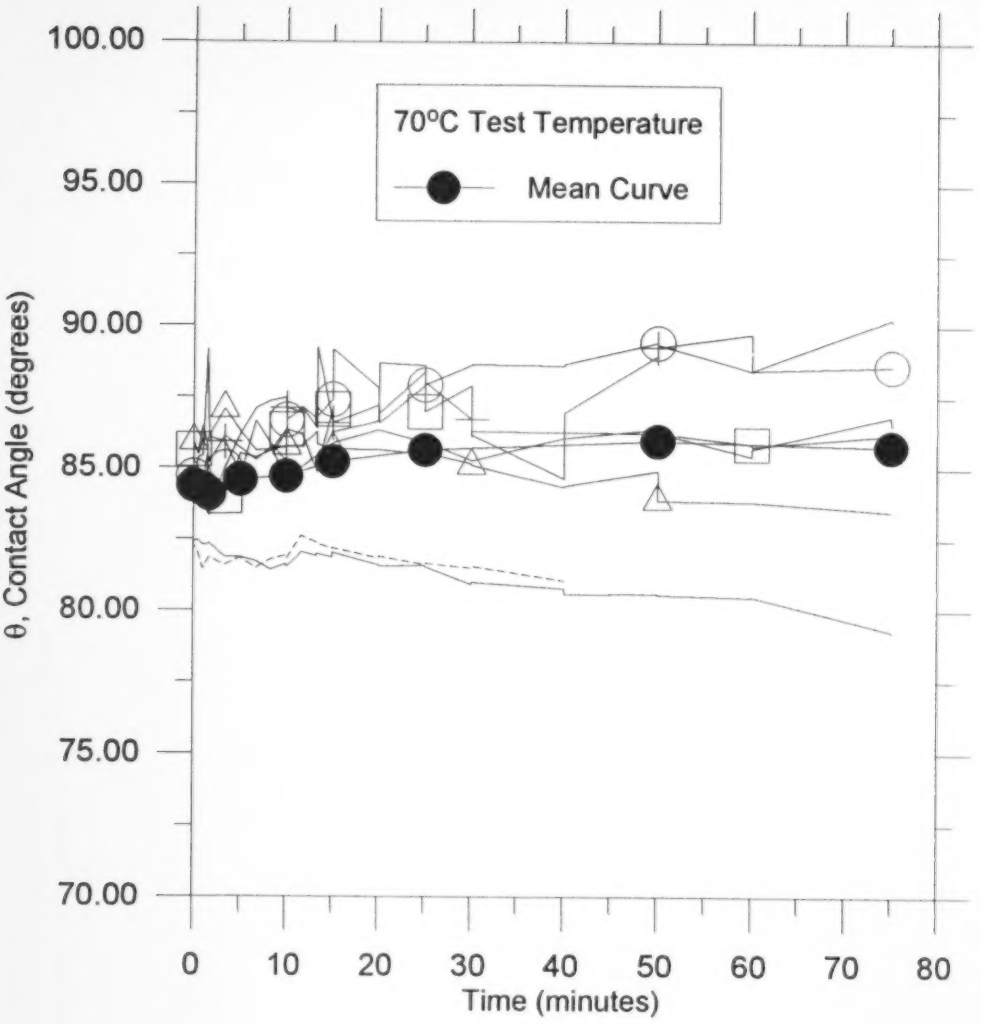

Figure 3.7: Time dependence of water-bitumen contact angle at 70°C.

REFERENCES

Alberta Oil Sands Technology and Research Authority, *The Thermodynamic and Transport Properties of Bitumens and Heavy Oils*, July 5, 1984.

Jasper, J.J., *Journal of Physical and Chemical Reference Data*, 1 (1972) 841.

Potoczny, Z.M, Vargha-Butler, E.I, Zubovits, T.K., and Neumann, A.W., *AOSTRA Journal of Research*, 1 (1984) 107.

CHAPTER 4

MODEL OF BITUMEN DROP - AIR BUBBLE ATTACHMENT

4.1 BITUMEN DROP - AIR BUBBLE MODEL FORMULATION

In order to analyze the stability of a bitumen drop - air bubble system in water under static conditions, a bitumen drop - air bubble attachment model was developed. The model assumes that a spherical drop of bitumen is in contact with a spherical air bubble as illustrated in Figure 4.1. The thermal and chemical equilibrium conditions are assumed constant, i.e., the temperature and chemical potential are constant through all phases in the system. The equilibrium configuration of this system can be derived by minimizing the total grand canonical free energy of the system [Callen, 1985; Li and Neumann, 1991].

The total grand canonical free energy, Ω, of the bitumen drop-air bubble-water system can be written as follows:

$$\begin{aligned} \Omega &= \Omega_w + \Omega_b + \Omega_a + \Omega_{wb} + \Omega_{wa} + \Omega_{ba} \\ &= -P_w V_w - P_b V_b - P_a V_a + \gamma_{wb} A_{wb} + \gamma_{ap} A_{wa} + \gamma_{ba} A_{ba} \end{aligned} \tag{4.1}$$

where the subscripts w, b, and a indicate the three bulk phases, water, bitumen, and air respectively; wb, wa, and ba indicate water-bitumen, water-air, and bitumen-air interfaces respectively; γ_{ap} is the apparent surface tension of the air bubble with a bitumen film. Consider that the volumes of the air bubble, bitumen drop, and water are constant. Minimization of the total free energy becomes:

$$d\Omega = \gamma_{wb} dA_{wb} + \gamma_{ap} dA_{wa} + \gamma_{ba} dA_{ba} \tag{4.2}$$

The surface areas, as shown in Figure 4.1, can be written as follows:

$$A_{wb} = 2\pi R_b^2 (1 + \cos\phi) \tag{4.3}$$

$$A_{wa} = 2\pi R_a^2 (1 + \cos\psi) \tag{4.4}$$

From geometry, it can be shown that the angle ψ is related to the angle ϕ by:

$$\psi = \sin^{-1}\left(\frac{R_b}{R_a}\sin\phi\right) \tag{4.5}$$

Therefore, the water-air surface area, Equation (4.4), can be rewritten as follows:

$$A_{wa} = 2\pi R_a^2 [1 + \cos(\sin^{-1}(\frac{R_b}{R_a}\sin\phi))] \tag{4.6}$$

The bitumen-air surface area can be written as follows:

$$A_{ba} = 2\pi R_b^2 (1 - \cos\phi) \tag{4.7}$$

Using Equations (4.3), (4.6), and (4.7) and minimizing the total grand canonical free energy with respect to ϕ gives:

$$\frac{d\Omega}{d\phi} = 2\pi R_b^2 \sin\phi (\gamma_{ba} - \gamma_{wb}) - \frac{2\pi R_b^2 \sin\phi\cos\phi\ \gamma_{ap}}{\sqrt{1 - (\frac{R_b}{R_a}\sin\phi)^2}} = 0 \tag{4.8}$$

A sessile air bubble on a bitumen surface surrounded by water is shown in Figure 4.2. For this system, the classical Young equation can be derived:

$$\gamma_{ap}\cos\theta = \gamma_{ba} - \gamma_{wb} \tag{4.9}$$

where θ is the water-bitumen contact angle. Substituting Equation (4.9) into Equation (4.8) and simplifying gives:

$$\cos\theta = \frac{\cos\phi}{\sqrt{1 - (\frac{R_b}{R_a}\sin\phi)^2}} \tag{4.10}$$

Rearranging this equation in terms of ϕ and simplifying results in the equation:

$$\cos\phi = \cos\theta \sqrt{\frac{1 - (\frac{R_b}{R_a})^2}{1 - (\frac{R_b}{R_a}\cos\theta)^2}} \tag{4.11}$$

The variable h in Figure 4.1 can be expressed as follows:

$$h = R_b(1 - \cos\phi) \tag{4.12}$$

The ratio of h over the radius of the bitumen drop, R_b, is a measure of the stability of the bitumen drop-air bubble attachment. As shown in Figure 4.1, as the ratio h/R_b increases, a larger portion of the bitumen drop is inside the air bubble, and hence the bitumen drop becomes more stably attached to the air bubble and is less likely to separate from the air bubble if agitated. This ratio can be written as:

$$\frac{h}{R_b} = 1 - \cos\theta \sqrt{\frac{1 - (\frac{R_b}{R_a})^2}{1 - (\frac{R_b}{R_a}\cos\theta)^2}} \qquad (4.13)$$

4.2 ATTACHMENT MODEL RESULTS

Equation (4.13) clearly shows that the attachment parameter, h/R_b, depends on two factors: the contact angle, θ, and the bitumen drop-air bubble size ratio, R_b/R_a. Figure 4.3 shows a plot of the ratio h/R_b for contact angles ranging from 0 to 90 degrees using radius ratios, R_b/R_a, ranging from 0 to 0.99. It can be seen from in this figure that at a given contact angle, as the radius ratio increases from 0 to 0.99, the ratio h/R_b increases , or system becomes more stable. This suggests that to enhance bitumen drop - air bubble attachment, the average size of the air bubbles should be the same as the average size of the bitumen drops.

The effects of the presence of a bitumen film on the bitumen drop - air bubble attachment are illustrated in Figures 4.4, 4.5, and 4.6. Since the contact angle is related to the surface tensions as shown by the classical Young equation, the ratio h/R_b given by Equation (4.13) can be plotted as a function of surface tensions. The values for the water-bitumen and bitumen-air surface tensions can be found in the literature [AOSTRA, 1984; Potoczny, 1984] . Using these values, combined with the measured time dependence of apparent surface tension, the ratio h/R_b can is plotted against time for room temperature, 50°C, and 70°C in Figures 4.4, 4.5, and 4.6. Also shown on these

figures is the ratio h/R_b assuming that no bitumen film was formed over the surface of the air bubble. In this case, the apparent surface tension would be the normal air-water surface tension found in the literature. Since all three interfacial tensions will be constant for this case, there is no time dependence for the no bitumen film lines shown in Figures 4.4, 4.5, and 4.6.

It can be seen from the difference between the bitumen film and no bitumen film lines in Figures 4.4, 4.5, and 4.6 that neglecting the bitumen film in the calculations results in an overestimation of the bitumen drop - air bubble attachment stability. This overestimation is more dominant for smaller radius ratios, or if the air bubble is much larger than the bitumen drop. Including the effects of a bitumen film of the air bubble surface reduces the stability or weakens the bitumen drop-air bubble attachment by approximately 5 to 10% for air bubbles much larger than the bitumen drops. For radius ratios closer to 1, the bitumen film reduces the stability of the system by approximately 1 to 4%.

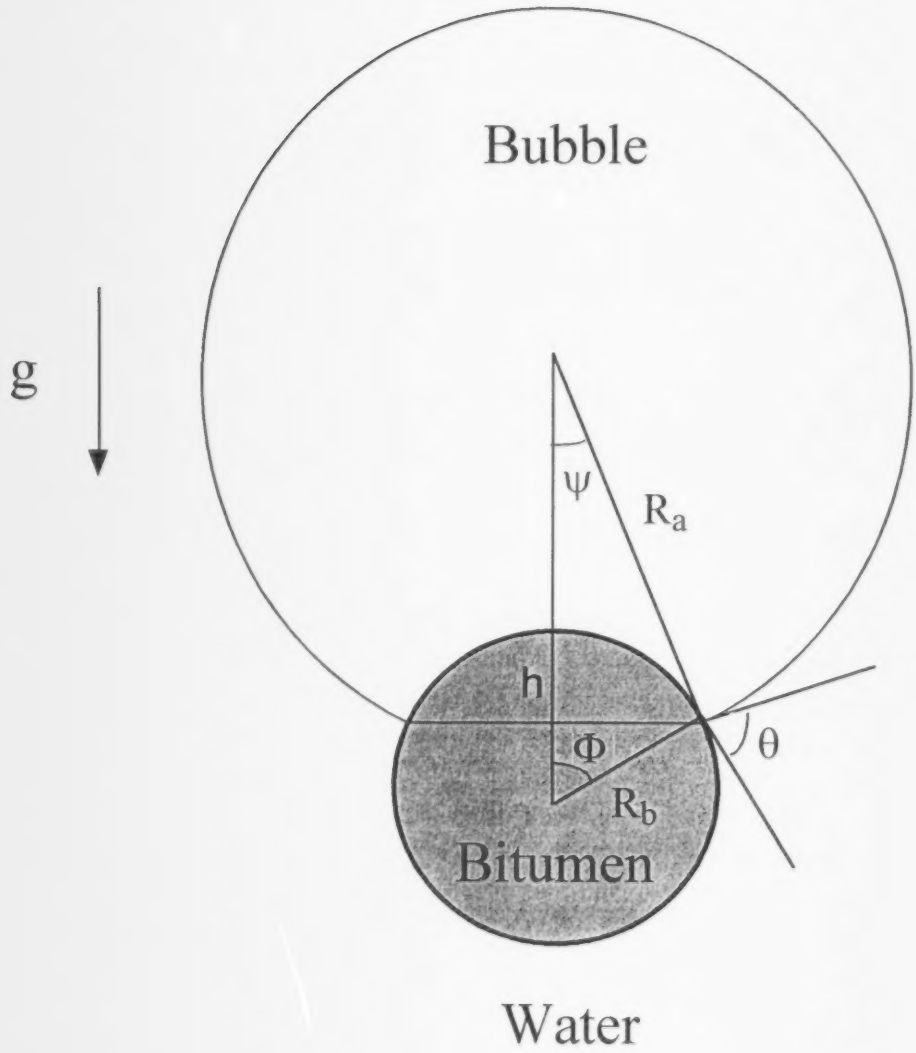

Figure 4.1: Bitumen drop - air bubble attachment model to predict stability.

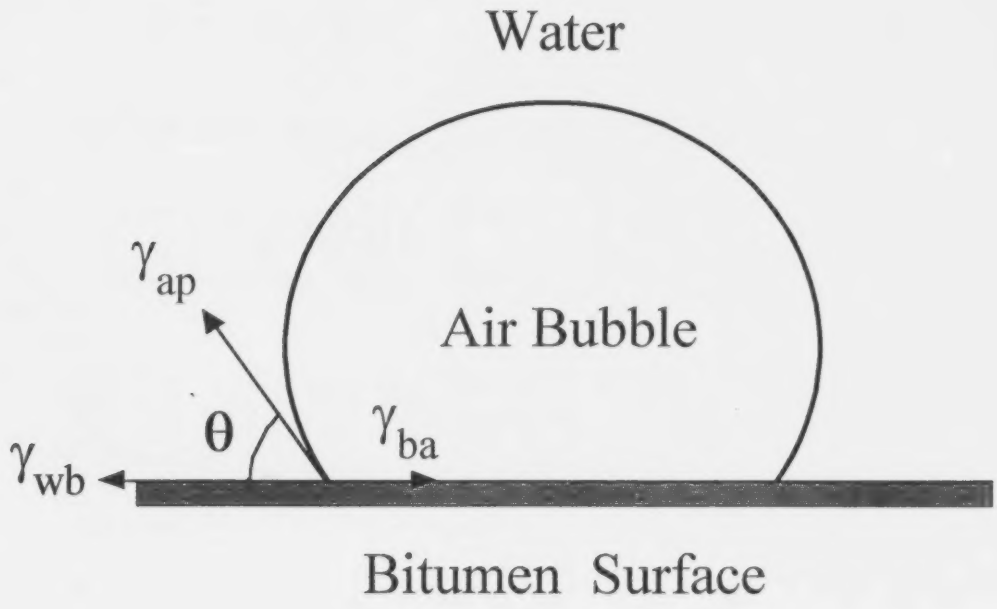

Figure 4.2: Side view of an axisymmetric air bubble on a bitumen coated surface.

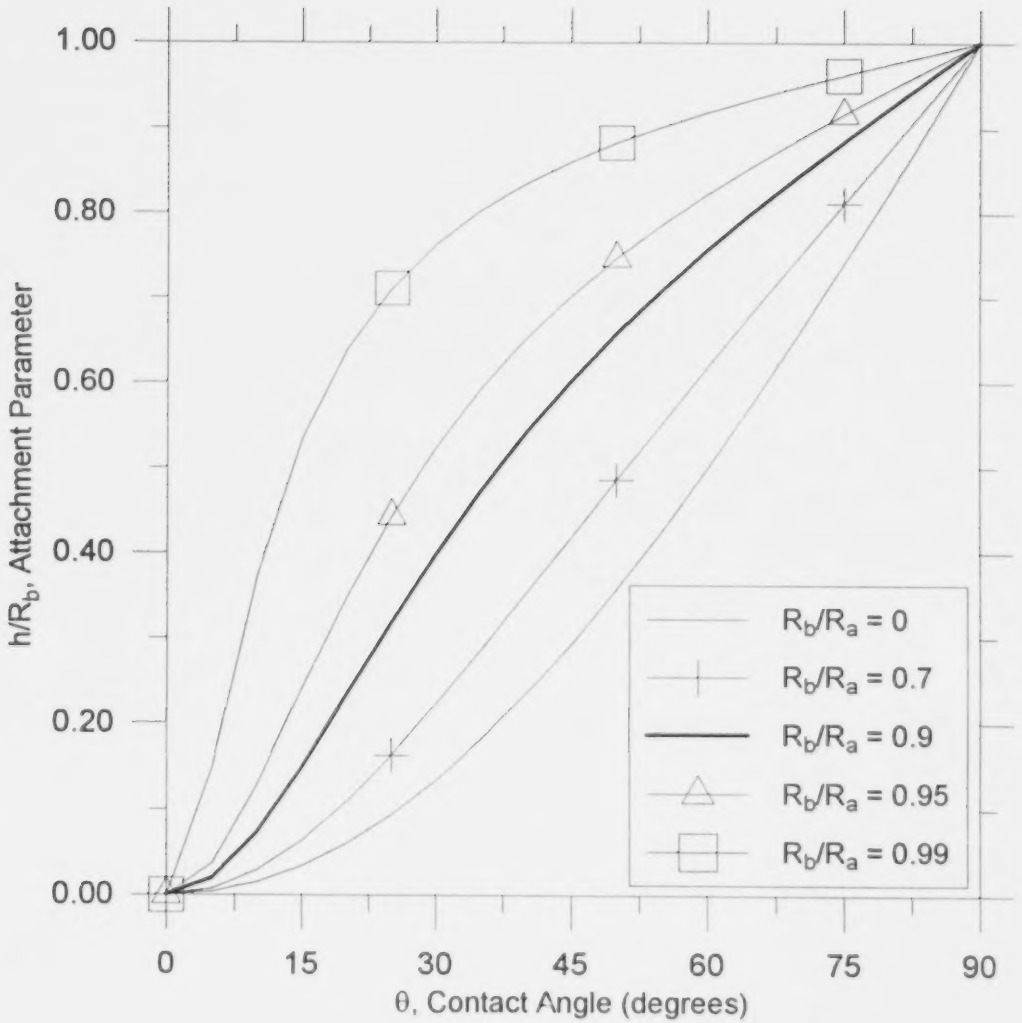

Figure 4.3: Bitumen drop - air bubble attachment parameter, h/R_b, as a function of water-bitumen contact angle.

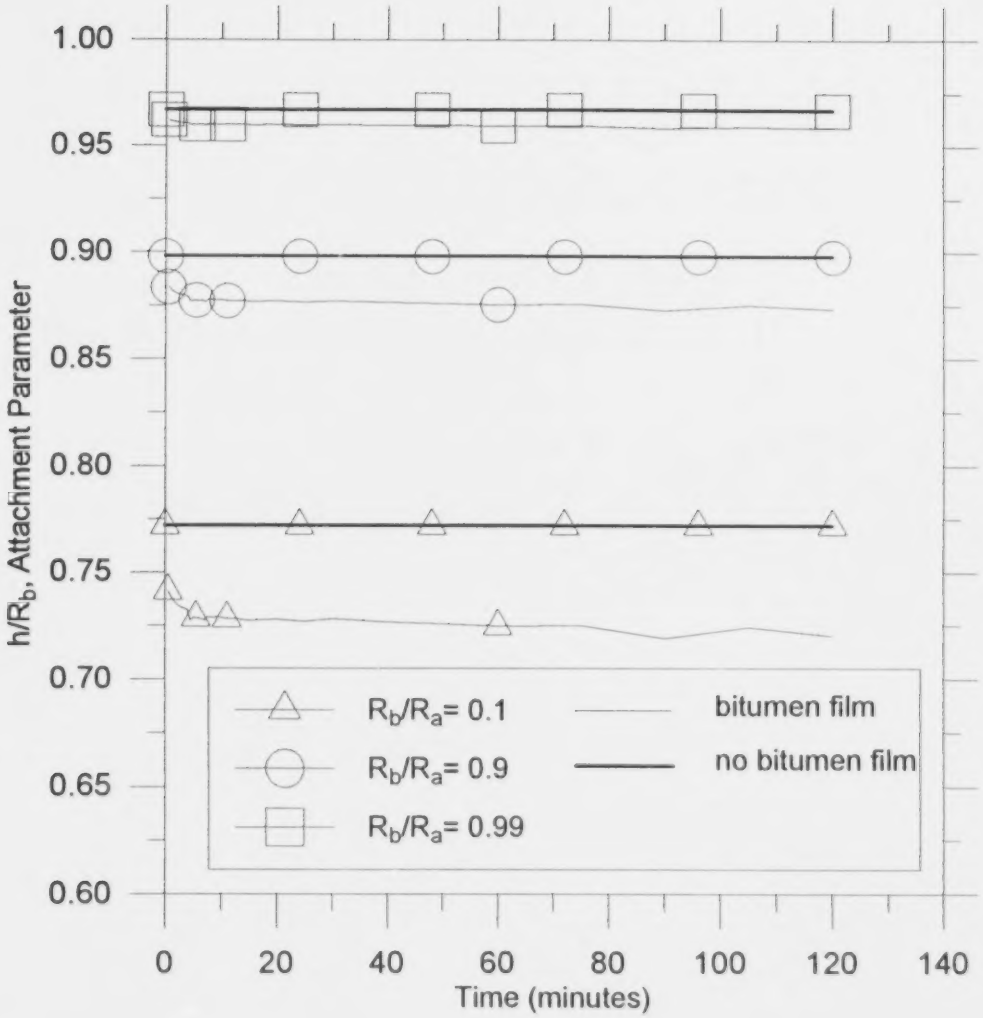

Figure 4.4: Effects of the bitumen film on bitumen drop - air bubble attachment at 23°C.

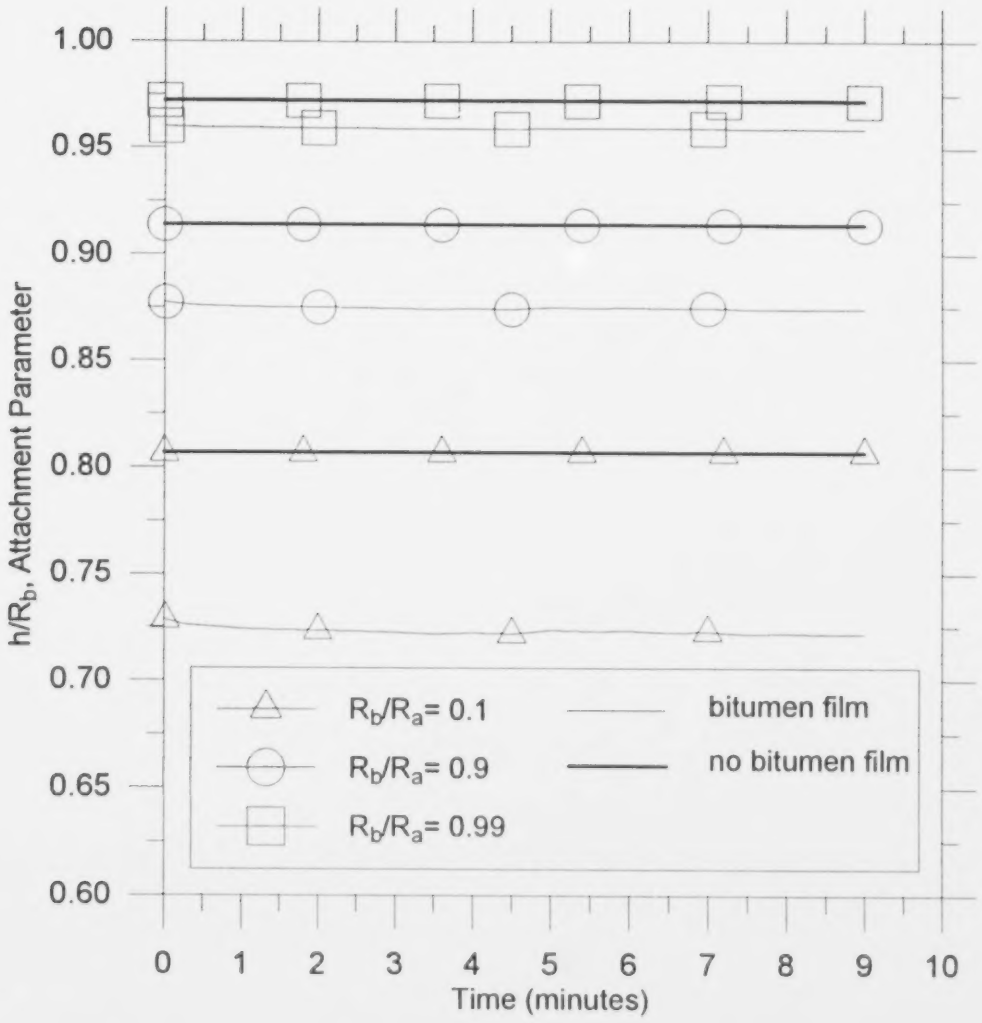

Figure 4.5: Effects of the bitumen film on bitumen drop - air bubble attachment at 50°C.

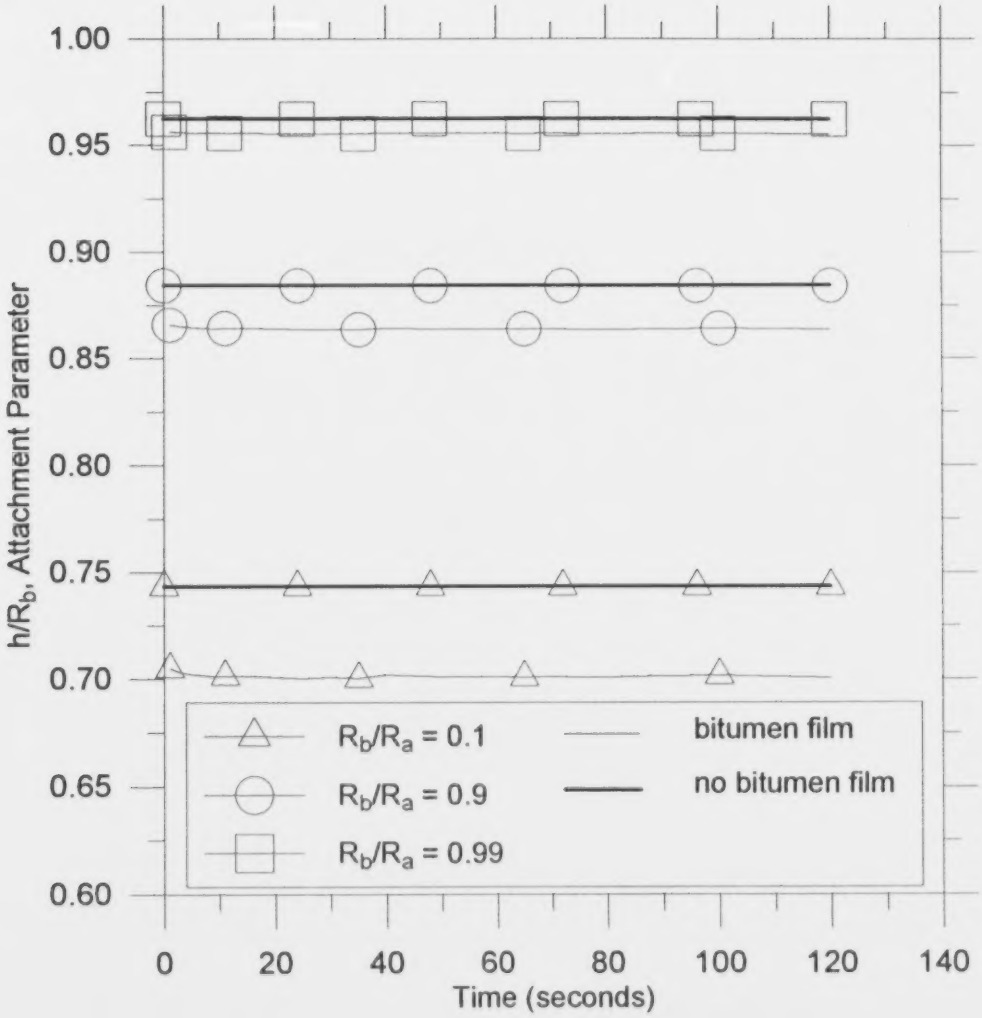

Figure 4.6: Effects of the bitumen film on bitumen drop - air bubble attachment at 70°C.

REFERENCES

Alberta Oil Sands Technology and Research Authority, *The Thermodynamic and Transport Properties of Bitumens and Heavy Oils,* July 5, 1984.

Callen, H.B., *Thermodynamics and an Introduction to Thermostatistics*, 2nd Edition, John Wiley & Sons, New York, 1985.

Li, D. and Neumann, A.W., *Advances in Colloid and Interface Science*, 36 (1991) 125.

Potoczny, Z.M, Vargha-Butler, E.I, Zubovits, T.K., and Neumann, A.W., *AOSTRA Journal of Research*, 1 (1984) 107.

CHAPTER 5

BITUMEN FILM THICKNESS MODEL

5.1 BITUMEN FILM THICKNESS MODEL FORMULATION

In this chapter, the interface separating an air bubble with a bitumen film surrounded by water is considered to have a finite thickness. A bitumen film theoretical model is developed in order to analyze the thickness of a bitumen film on an air bubble surface. The model assumes that a spherical air bubble surface is covered with a bitumen film of thickness h_f as shown in Figure 5.1. Since the bitumen film is considered to be a bulk phase, there are two interfaces shown in this figure: water-bitumen and bitumen-air. Two equations can be written using the Laplace equation of capillarity to describe these two interfaces:

$$P_a - P_b = \gamma_{ba} J_{ba} \tag{5.1}$$

$$P_b - P_w = \gamma_{wb} J_{wb} \tag{5.2}$$

where P_a, P_b, and P_w are the pressures of the air, bitumen, and water phases respectively. γ_{ba} and γ_{wb} refer to the bitumen-air and water-bitumen surface tensions. J_{ba} and J_{wb} refer to the mean curvatures of the bitumen-air and water-bitumen interfaces. ADSA-P measures the surface tension of the bubble by taking an image of the bubble profile, or view of the bubble's outer surface. The Laplace equation used by the ADSA-P technique to calculate the apparent surface tension, γ_{ap}, can be written as follows:

$$P_a - P_w = \gamma_{ap} J_{wb} \tag{5.3}$$

Adding equations (5.1) and (5.2) and equating them to (5.3) gives:

$$\gamma_{ba} J_{ba} + \gamma_{wb} J_{vb} = \gamma_{ap} J_{wb} \tag{5.4}$$

Rearranging this equation gives:

$$\frac{J_{ba}}{J_{wb}} = \frac{\gamma_{ap} - \gamma_{wb}}{\gamma_{ba}} \tag{5.5}$$

If spherical surfaces are assumed, the mean curvatures can be written as follows:

$$J_{ba} = \frac{2}{R_a} \tag{5.6}$$

$$J_{wb} = \frac{2}{R_{wb}} = \frac{2}{R_a + h_f} \tag{5.7}$$

where R_a, R_{wb}, and h_f refer to the radius of the air bubble, the radius to the water-bitumen interface, and the thickness of the bitumen film. Equation (5.5) can then be rewritten using (5.6) and (5.7) as:

$$\frac{R_a + h_f}{R_a} = \frac{\gamma_{ap} - \gamma_{wb}}{\gamma_{ba}} \tag{5.8}$$

Equation (5.8) can then be rearranged as:

$$\frac{h_f}{R_a} = \frac{\gamma_{ap} - \gamma_{wb} - \gamma_{ba}}{\gamma_{ba}} \tag{5.9}$$

Equation (5.9) shows that the equilibrium ratio of the film thickness to the radius of the air bubble is a function of the apparent, water-bitumen, and bitumen-air surface tensions.

If these three surface tensions are known, the film thickness as related to air bubble size can be solved.

Trends over time such as increasing film thickness or decreasing bubble size can also be formulated using the above analysis. Equation (5.2) can be used to show how the radius of the air bubble changes over time. Equation (5.2) can be rewritten as:

$$P_b - P_w = \gamma_{wb} J_{wb} = \frac{2\gamma_{bw}}{R_a + h_f} \tag{5.10}$$

In the experiments, the temperature and pressure of the water phase remained constant. Since the bitumen film was in contact with a reservoir of bitumen with a constant pressure on the tip of the teflon needle and the volume of the bitumen film was allowed to expand on the air bubble surface, it is assumed that the pressure of the bitumen film is constant. If it is also assumed that the water-bitumen surface tension is constant with respect to time, t, then the following equations can be written:

$$\frac{dP_b}{dt} = 0 \tag{5.11}$$

$$\frac{dP_w}{dt} = 0 \tag{5.12}$$

$$\frac{d\gamma_{wb}}{dt} = 0 \tag{5.13}$$

Taking a derivative of equation (5.10) with respect to time and substituting equations (5.11), (5.12), and (5.13) gives:

$$- \frac{2\gamma_{bw}}{(R_a + h_f)^2} \left(\frac{dR_a}{dt} + \frac{dh_f}{dt}\right) = 0 \qquad (5.14)$$

Since water-bitumen surface tension in not zero:

$$\gamma_{wb} \neq 0 \qquad (5.15)$$

then for equation (5.14) to be zero, the following has to be true:

$$\frac{dR_a}{dt} = - \frac{dh_f}{dt} \qquad (5.16)$$

As shown in equation (5.16), the rate of change of the air bubble radius with respect to time is opposite to the rate of change of the film thickness with respect to time. From experimental observations during the measurement of the apparent surface tension, it is known that the film thickness increases over time. Since:

$$\frac{dh_f}{dt} > 0 \qquad (5.17)$$

Equation (5.16) shows that if the bitumen film thickness increases over time, then the following must be true:

$$\frac{dR_a}{dt} < 0 \qquad (5.18)$$

This equation shows that if the bitumen film thickness increases over time then the radius of the air bubble decreases over time. This result concurs with the experimentally observed trend that the bitumen film thickness increases and the radius of the air bubble decreases over time.

5.2 BITUMEN FILM MODEL RESULTS

Equation (5.9) shows the ratio of film thickness to air bubble size as a function of surface tensions. Using published values of γ_{ba} [Potoczny et al., 1984] and γ_{wb} [AOSTRA, 1984] along with the experimentally determined values of γ_{ap} as discussed in Chapter 3, the film thickness can be determined. Table 5.1 shows the published and experimentally determined surface tension values.

Table 5.1: Surface tension values used to calculate film thickness.

	γ_{ap} (mJ/m^2)	γ_{ba} (mJ/m^2) [Potoczny, 1984]	γ_{wb} (mJ/m^2) [AOSTRA, 1984]
23°C	60.7 ± 1.4	33.3 ± 0.3	18.1 ± 4.0
50°C	57.4 ± 0.9	31.2 ± 0.27	11.4 ± 4.0
70°C	56.3 ± 0.3	29.7 ± 0.26	6.3 ± 4.0

The equilibrium ratio of bitumen film thickness to air bubble radius at the temperatures of 23°C, 50°C, and 70°C can be calculated by using Equation (9) along with the surface tension values shown in Table 5.1. The resulting equilibrium ratios are shown in Table 5.2:

Table 5.2: Equilibrium bitumen film thickness to air bubble radius ratio.

	23°C	50°C	70°C
Equilibrium h_f/R_a	0.28 ± 0.14	0.47 ± 0.14	0.68 ± 0.15

As can be seen in Table 5.2, the ratio of film thickness to air bubble size increases with increasing temperature which agrees with experimental observations. For a given air bubble radius, the film at 50°C is 1.7 times as thick and at 70°C is over twice as thick as a film at room temperature. These values represent a 68% and 143% increase in bitumen thickness for 50°C and 70°C respectively over room temperature. This table shows that the thickness of the bitumen film can either be increased by increasing the temperature or increasing the size of the air bubble.

5.3 COMPARISON OF BUBBLE ATTACHMENT AND BITUMEN FILM THICKNESS MODELS

The results from the above section indicate that since the ratio h_f/R_a is fixed for a given temperature, a thicker bitumen film will require an air bubble with a larger radius. This would seem to indicate that to achieve greater bitumen recovery per air bubble, the air bubbles should be very large. This can be compared with the results in Chapter 4 which predicted that the air bubble should be smaller to promote greater

stability of the bitumen drop - air bubble attachment. The results, as discussed in Chapter 4, indicated that the air bubble and the bitumen drop should be the same size to have the maximum stability. These two models predict the trends which are typically seen in industry. Bubbles are reduced in size to increase the stability of the bitumen drop - air bubble attachment at the expense of the amount of bitumen carried by each air bubble. There must be a compromise between bubble stability and film thickness to produce an optimum air bubble size to use in the secondary recovery stage of the Hot Water Extraction Process.

In industry, the typical air bubble radius varies between 0.1 and 1 mm. The typical radius of a bitumen drop varies between 0.01 and 0.1 mm. Using the results of the Bubble Attachment Model in Chapter 4, the smallest air bubble radius of 0.1 mm would promote the greatest attachment stability between the air bubble and bitumen drop. Using the air bubble radius, R_a, of 0.1 mm with the results for the equilibrium ratio, h_f/R_a, the following results for equilibrium bubble film thickness are obtained as shown in Table 5.3:

Table 5.3: Equilibrium bitumen film thickness assuming an air bubble radius of 0.1 mm.

	23°C	50°C	70°C
Equilibrium h_f	0.028 ± 0.014	0.047 ± 0.014	0.068 ± 0.015

The results shown in Table 5.3 obviously show the same trends shown in Table 5.2. The bitumen film thicknesses at 50°C and 70°C are 1.7 and 2.4 times as thick as a film at room temperature. The results shown in Table 5.3 agree with the experimentally observed trends that the bitumen film thickness on the air bubble surface increased with increasing temperature.

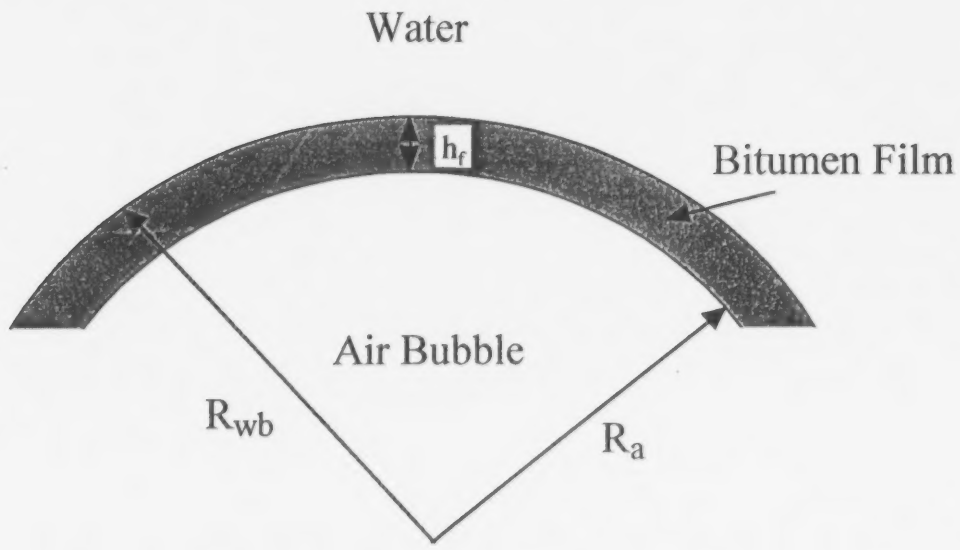

Figure 5.1: Two interfaces formed by a bitumen film of thickness h_f on an air bubble surface in water.

REFERENCES

Alberta Oil Sands Technology and Research Authority, *The Thermodynamic and Transport Properties of Bitumens and Heavy Oils*, July 5, 1984.

Potoczny, Z.M, Vargha-Butler, E.I, Zubovits, T.K., and Neumann, A.W., *AOSTRA Journal of Research*, 1 (1984) 107.

CHAPTER 6

SUMMARY

6.1 SUMMARY OF EXPERIMENTAL AND MODEL RESULTS

The experimental data for the tim and temperature dependence of apparent surface tension and contact angle of an air bubble with a bitumen film at 23°C, 50°C, and 70°C along with the bitumen drop-air bubble attachment and bitumen thickness models can be summarized as follows:

1. Due to the formation of a bitumen film on an air bubble surface, the apparent bubble surface tension initially decreases rapidly and gradually reaches an equilibrium value. At 70°C, for example, the equilibrium value of the apparent surface tension is approximately 9 mJ/m^2 or 14% less than the water-air surface tension.

2. The time required for the complete formation of the film is shorter for higher temperatures. The time to reach equilibrium was reduced from approximately 11 minutes to 7 seconds or 99% from room temperature to 70°C.

3. Measured contact angles at room temperature and 50°C were 11% and 13% higher than theoretically determined contact angles using the Young Equation. Although the same bitumen was not used in the experiments as was used to determine theoretical

numbers, the results show that the measured and theoretical contact angles are in reasonable agreement.

4. In comparison with the case of no bitumen film on air bubbles, the bitumen film formed on an air bubble surface weakens the bitumen-bubble attachment by 1 to 10% depending on the bitumen drop-air bubble size ratio.

5. As the bitumen drop to air bubble radius ratio, R_b/R_a, increases from 0 to 1, the attachment parameter, h/R_b, indicates increasing stability of the bitumen drop-air bubble attachment. In order to enhance the bitumen drop-air bubble attachment, the average size of air bubbles should be the same as the average size of bitumen drops.

6. The bitumen film theoretical model predicts that the ratio of bitumen thickness to air bubble radius is a function of the water-bitumen, bitumen-air, and apparent surface tensions. Using published values of water-bitumen and bitumen-air surface tensions along with experimentally determined values for apparent surface tensions, it was calculated that for a constant radius air bubble, the film was 1.7 and 2.4 times as thick at 50°C and 70°C respectively than at room temperature.

6.2 FUTURE WORK

The experimental and theoretical model results show that higher temperatures promote greater bitumen recovery in the secondary recovery stage of the Hot Water

Extraction Process to recover bitumen from oil sands. Current operations are carried out at approximately 80°C, but industry is tending towards carrying out this process at lower temperatures to reduce operational heating costs. Ideally, the process would be carried out at room temperature to avoid any expensive heating operations. Without the benefit of high temperatures to promote greater bitumen film thickness, the size of the air bubbles and bitumen drops may become more critical. Factors such as pH and salt concentration will also have to be considered and tested to study the effects of these parameters on apparent surface tension and contact angle.